Evaluation of cloud and photolysis treatment in two coupled Chemistry-Climate Models and their subsequent effects on atmospheric composition

CID: 00732524
Supervisor: Dr Apostolos Voulgarakis
Assessor: Professor Joanna D. Haigh
Word Count: 9716

Declaration

Both students contributed equally to the analysis, splitting the job so that each of them worked on output from different composition-climate models. The data existed before the students started, or was provided by modellers while the project was evolving. However, the main challenge of the students was not to produce the data but to analyse a large volume of it in suitable and useful ways. When the students started, there were some programs from previous projects that were used as templates to start from. The students used these programs as a basis to produce their own programs for examining the aspects of this topic that we discussed and those that they thought would be interesting to explore. They also wrote some of their own programs. Apart from me, the students received some assistance by one PhD student from my group, but that was only occasional and only restricted to providing some advice (not e.g. writing programs for them etc). Neither Student 00729330 nor Student 00732524 have worked on this topic or generally in SPAT before, so the MSci project cannot be considered as an extension of summer work/essay projects.

Contents

1. Abstract

This project aims to evaluate the treatment and implementation of clouds as well as calculation of photolysis rates in two Chemistry-Climate models participating in the Chemistry-Climate Model Initiative (CCMI), namely the Goddard Earth Observing System Chemistry-Climate model (GEOSCCM) and the ECHAM/MESSy Atmospheric Chemistry model (MESSy). GEOSCCM was found to have a global systematic low bias in total cloud fraction of ~20-50% compared to satellite retrieval products from the International Satellite Cloud Climatology Project (ISCCP). MESSy total cloud fractions are consistent with ISCCP within the range of known uncertainties for ISCCP dataset values (~10%). However the low bias does not affect the expected vertical profile of correlations between clouds and $J(NO_2)$ rates in GEOSCCM, nor does it affect expected correlations between clouds and $J(O^1D)$. The latter is found to be affected more by prominent long term trends in $J(O^1D)$, specifically a decreasing boundary layer trend was found over India accompanied by an increasing trend in tropospheric O_3 over the same region in GEOSCCM, neither of which were present in MESSy. It is proposed that this is due to omission of time-varying surface layer aerosol emissions from photolysis rate calculations in MESSy. MESSy is listed as using an interactive online photolysis scheme, however it is proposed that taking into account time-varying aerosols should be a requirement for this as not doing so can possibly lead to omission of a significant regional source of tropospheric O_3. 2D and 3D cloud variables using the 2.5°/2° Lon/Lat resolution contain low biases in GEOSCCM which is likely a deficiency in cloud representation and not implementation.

2. Introduction

Atmospheric chemistry is affected by clouds through a number of well-known dynamical and radiative processes. The former processes include vertical transport of chemicals from the boundary layer due to convective clouds (Fanyou et al, 1993), Lightning produced NO_x species as a result of storm clouds (Tie et al, 2002) as well as wet removal of chemicals due to precipitation (Tie et al, 2003). Clouds affect the energy budget (due to alteration of longwave radiation) as well as having significant effects on tropospheric photochemistry due to scattering and attenuation of shortwave radiation which impacts photolysis rates (Tie et al, 2003). Photolysis is one of the key radiative processes that governs tropospheric chemistry and the production of stratospheric O_3. The dependence on the availability of light introduces complexity when considering scattering due to clouds in radiative transfer calculations. Treatment of clouds and aerosols contribute the largest uncertainty to estimates of Earth's changing energy budgets (IPCC 5th report, 2013) and photochemistry contributes to this. It is therefore important to continue to understand and improve treatment of clouds and photolysis in modern CCMs.

3. Theory

To quantify cloud alteration of photolysis rates and its subsequent effects on atmospheric composition, we will focus on the main photolysis reactions that occur in the troposphere and observe the effects of altering these reactions on tropospheric and stratospheric chemistry in particular.

3.1 Tropospheric O_3

Photolysis plays an important role in driving both the (indirect) production and destruction of O_3 in the troposphere. O_3 is a toxic pollutant and is an important greenhouse gas which contributes to climate forcing. The main two reactions responsible for the production of tropospheric O_3 are

$$NO_2 + h\nu\ [\lambda < 420nm] \rightarrow NO + O(^3P) \tag{3.1}$$

$$O_2 + O(^3P) \rightarrow O_3 \tag{3.2}$$

where reaction (3.1) demonstrates the photolysis of NO_2 producing an NO molecule and an oxygen atom, the latter of which subsequently combines with existing O_2 molecules in the air to form O_3. Reaction (3.2) is responsible for O_3 production in both the troposphere and the stratosphere (Madronich, 1993), however the latter is governed by the Chapman mechanism which produces the $O(^3P)$ atom via O_2 photolysis requiring light of wavelengths $\lambda < 240$nm which isn't available below the stratosphere (Jacob, 1999). It can be seen that both NO and NO_2 (together referred to as NO_x) molecules are important precursors to O_3 production. O_3 is removed from the troposphere via photolysis according to reaction (3.3) below which results in the production of an excited oxygen atom, the reactions are as follows.

$$O_3 + h\nu\ [\lambda < 330nm] \rightarrow O_2 + O(^1D) \tag{3.3}$$

$$O(^1D) + H_2O \rightarrow 2OH \tag{3.4}$$

In reaction (3.4), the excited oxygen atom combines with water molecules in the air resulting in the production of two OH molecules. This is significant as OH is the main oxidant that is responsible for removing greenhouse and toxic combustion gases such as CH4 and CO from the atmosphere, particularly in the troposphere as these gases are generally emitted at the surface (Jacob, 1999). This is the main mechanism which allows photolysis to significantly impact atmospheric composition.

3.2 OH molecule and the null cycle

OH lifetimes in the atmosphere is of the order of one second, as a result of this, atmospheric concentrations of OH respond rapidly to changes in sources or sinks (Jacob, 1999). It is therefore useful to monitor global distribution and concentrations of OH in the atmosphere as an indicator of local variations of its precursors namely H_2O and O^1D, the latter of which depends on variations in levels of light (this will be discussed further in section (3.3)).

The OH molecule is the main oxidizer of the troposphere and proceeds to oxidize chemical species such as the aforementioned CO and CH4 (for which OH is the main sink) and also other Volatile Organic Compounds (VOC's). This produces peroxy radicals which subsequently recycle NO molecules back to NO_2 allowing reaction (3.1) to restart O_3 production. The process

encompassing all of this is known as the null cycle (Jacob, 1999) and one such reaction involving CO is shown below

$$OH + CO + O_2 \rightarrow CO_2 + HO_2 \quad (3.5)$$

$$NO + HO_2 \rightarrow NO_2 + OH \quad (3.6)$$

Where the HO_2 molecule is the produced hydrogen based peroxy radical which recycles NO back to NO_2 via reaction (3.6). There are many factors that can affect the concentrations of the chemical species involved in reactions (3.1) – (3.4). This can alter reaction rates and lead to disturbances of the null cycle. Such factors include anthropogenic injections of CH4, CO and NO_x into the atmosphere which causes over recycling of NO to NO_2 resulting in a net production of ozone. Lightning events can also inject NO_x into the atmosphere which causes similar effects (Tie et al, 2002). More relevant to our project however, is the fact that the rates of the above reactions heavily depend on the levels of light present in the atmosphere which in turn also affects the null cycle. It is this that we will focus on as it is the main factor that is affected by the radiative properties of clouds.

3.3 Photolysis rate coefficient

The rate at which photolysis occurs for the above reactions is defined by the parameter J_A (often called J value) which is the photolysis rate coefficient of molecule A and has units of s^{-1}. It is calculated as follows

$$J_A = \int_0^\infty \sigma_A(\lambda)\varphi_A(\lambda)F_A(\lambda)\, d\lambda \quad (3.7)$$

where σ_A is the absorption cross section of molecule A, φ_A is the quantum yield of molecule A and F_A is the actinic flux incident on the molecule, all exhibiting a wavelength dependence λ. The first two variables are probability quantities (respectively, the probability of photon absorption and the absorption event causing disassociation) and can be experimentally determined in laboratory conditions for a given molecule, whereas the actinic flux (total number of photons passing through a unit horizontal area per unit time) incident on such a molecule varies depending on local light intensity which in turn can be affected in the atmosphere by factors such as the solar zenith angle and absorption/scattering due to clouds.

In the atmosphere, variations in the photolysis rate of NO_2 and O_3 to O^1D (hereafter referred to as $J(NO_2)$ and $J(O^1D)$ respectively) is mainly caused by local variations of actinic flux available to the two molecules, therefore it is this quantity that is affected by the radiative properties of clouds. The quantum yield φ_A for $J(O^1D)$ has an additional significant temperature dependence (increases with temperature) for ranges found in the troposphere which means $J(O^1D)$ should also decrease noticeably with altitude. Also $J(O^1D)$ is strongly dependent on the stratospheric ozone column (where O_3 is abundant) and thus falls off rapidly with solar zenith angle. (Jacob, 1999; Wild et al, 2000).

In summary, it is useful to observe global distributions and values of $J(NO_2)$ and $J(O^1D)$ along with global concentrations of OH in order to monitor effects of clouds on photolysis and their subsequent effects on atmospheric chemistry and this is indeed what we will focus on.

3.4 Radiative properties of clouds

When solar radiation is incident on clouds from above, there is an enhancement of actinic flux above clouds due to backscattering of radiation, and a reduction of actinic flux below due to attenuation and scattering of radiation as light makes its way through the clouds. This will cause an enhancement and reduction of $J(NO_2)$ and $J(O^1D)$ accordingly and will go on to affect concentrations of O_3 and OH as described above. This effect is demonstrated well in figure 1 by Tie et al, (2003) which shows the aforementioned effects for $J(O^1D)$.

The scattering particles in clouds are cloud droplets which are water particles particularly in liquid and ice phases. Liquid water cloud droplets are large and scatter light with as much as half of their scattering in the forward direction within a few degrees of the original beam (Wild et al 2000). These large particles scatter light across the entire UV-visible wavelength spectrum almost equally according to Mie theory and appear white or grey corresponding to how clouds appear in the sky (Wild et al, 2000). Ice clouds with large multi-edged crystals scatter light differently than Mie theory water clouds and thus scattering events from these types of clouds must be treated differently (Wild et al, 2000)

How models treat these cloud-related scattering events, as well as scattering from other particles that exist in the air such as aerosols, depends on the setup of each individual model and treatment is likely to be different and unique between models. This introduces uncertainties in the quantitative effects that clouds have on atmospheric photochemistry and is one of the key reasons why there are conflicting conclusions on how much clouds affects global concentrations of chemical species such as tropospheric O_3 (Tie et al, 2003; Liu et al, 2006).

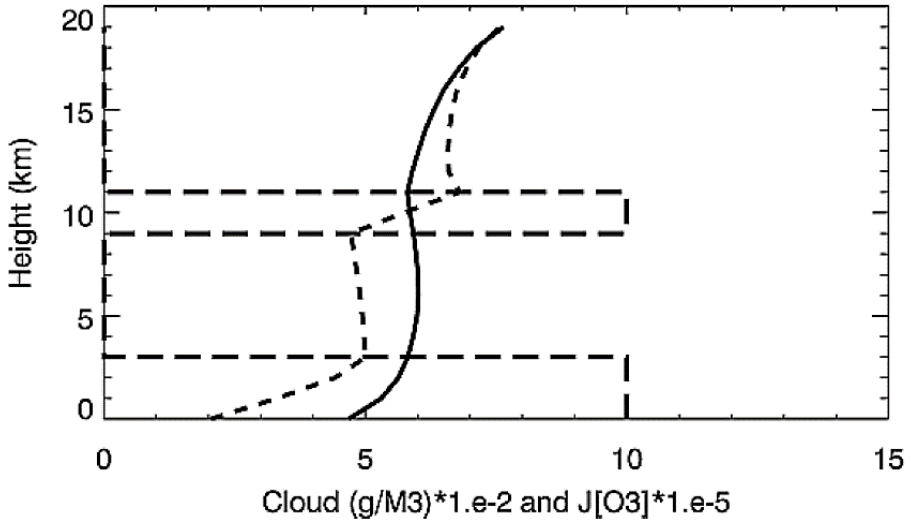

Figure 1 – Model calculated $J(O^1D)$ rates from Tie et al, (2003) using a simplified radiative transfer model. Increase and decrease in $J(O^1D)$ above and below the two vertical cloud distributions are a result of backscattering and attenuation of solar radiation. The long dashed lines show the vertical location of the cloud layers, the short dashed lines represent the modelled $J(O^1D)$ values with the clouds included and the solid line represents the modelled $J(O^1D)$ values without clouds.

The main parameter that quantifies the radiative properties of clouds is its cloud optical depth parameter τ. This is defined as an integrated extinction coefficient of radiation over a vertical column of unit cross section, where the extinction coefficient is the fractional depletion of radiation per unit path length (GES DISC, 2016). The unit cross-sectional area and vertical extent of the atmosphere depends on the level of resolution of 3D space that a CCM provides and the exact parameterization and implementation of τ is unique and usually different depending on the model used. This leads to further differences in quantifying cloud effects on photolysis and will be considered later when diagnosing differences between model data.

Tropospheric $J(NO_2)$ reactions occur in the wavelength range ($290nm \leq \lambda \leq 420nm$) whereas tropospheric $J(O^1D)$ occurs for ($290nm \leq \lambda \leq 330nm$) where light of wavelengths below the lower limit does not penetrate into the troposphere (Jacob, 1999). As a result, $J(NO_2)$ is less affected by Rayleigh scattering and is independent of O_3 absorption as opposed to $J(O^1D)$ which is dependent on these as well as factors mentioned previously such as the solar zenith angle (Wild et al, 2000). Therefore even though Mie scattering is effectively independent of wavelength, it is expected that water cloud scattering should be more prominent for $J(NO_2)$ compared to $J(O^1D)$ in the troposphere (the former also occurs in the visible wavelength regime for which solar intensity is slighter higher).

4. Model descriptions

The data used for this project are outputs of hindcast simulations from two coupled Chemistry-Climate models participating in CCMI. Coupled Chemistry-Climate Models (CCMs) are a new generation of atmospheric models that represents both stratospheric chemistry and atmospheric climate. The coupling of the two processes in a single model allows the study of feedback processes between the two (Morgenstern et al, 2010). This allows for more in-depth studies on how boundary layer processes and chemistry can affect composition in upper layers of the atmosphere. CCMs have spatially defined 3D grid-boxes of varying resolution and temporally simulate both hindcast and forecast projections of atmospheric data.

Outputs from ECHAM/MESSy atmospheric chemistry model (MESSy) and Goddard Earth Observing System Chemistry-Climate Model (GEOSCCM) was used in the analysis for this project. There are several key components to CCMs all of which handle different physical and chemical processes and these are all linked by feedback processes, however only a few of the components are relevant to clouds effects on photolysis rates. The relevant components as well as the two model's treatment of these components will be discussed below.

4.1 - Photolysis schemes

The radiative transfer scheme used for calculating photolysis rates throughout the atmosphere is a subset of one of the radiative processes handled by the dynamical core of a CCM (the other pertaining to longwave heating). Inspection of the models participating in CCMI show substantial differences in the treatment of radiative transfer schemes used for photolysis (hereafter referred to as photolysis scheme) (Morgenstern et al, 2010). In the past, photolysis rates were not calculated online, meaning that photolysis rates in time and space were non-interactive with physical processes such as cloud cover and aerosol concentrations due to impractically excessive computation times. Offline photolysis rates were calculated under average conditions and tabulated for use online (Telford et al, 2013). However, presently it is increasingly common for CCMs to employ interactive photolysis schemes that do take into account such processes and this is the case for both MESSy and GEOSCCM.

4.2 - JVAL

JVAL is the name of the photolysis scheme used in MESSy. Landgraf and Crutzen (1998) created an efficient method for online calculation of J values which was used in several atmospheric models. Joeckel et al, (2005) then subsequently adapted this for use in MESSy (Sander et al, 2014). In the model, the integral in equation (3.7) used to calculate photolysis rates is approximated as the sum

$$J_A = \sum_{i=1}^{N} \sigma_A(\lambda)\varphi_A(\lambda)F_A(\lambda)\,\Delta\lambda_i \qquad (4.1)$$

where the spectrum is divided into N wavelength bins and σ_A, φ_A and F_A are average values in the bins of size $\Delta\lambda$. To obtain accurate photolysis rate calculations, N has to be large, however this renders computation times excessive. Thus the spectrum is split into 8 photochemically active wavelength bins and the sum is further reduced such that photolysis rates are calculated as prescribed by Sander et al, (2014) via equation (4.2)

$$J_A \approx \sum_{i=1}^{8} J_{i\ A}^{a} \times \sigma_i \qquad (4.2)$$

where $J_{i\ A}^{a}$ is the J value for molecule A in a purely absorbing atmosphere and is pre-calculated, whereas σ_i is a factor which takes into account the influence of scattering by air, aerosol and cloud particles and is calculated during runtime, thus encapsulating the interactive element of MESSy's photolysis scheme (Sander et al, 2014). σ_i depends on the absorption and scattering optical depths of clouds and aerosols as well as the asymmetry factor of their scattering phase function (the angular distribution of scattered light intensity). The exact parameterization of σ_i is beyond the scope of this project (for this, the reader is referred to Landgraf and Crutzen, 1998) however, the main differences between the photolysis schemes used in the two CCMs as a result of use of this parameter will be discussed later on.

Table 1 from Sander et al, (2014) shows the 8 spectral wavelength bands used in photolysis calculations for JVAL. For the spectral bands with wavelengths λ>202.0 nm, scattering by air molecules, aerosols and cloud particles are significant and thus σ_i is calculated for these wavelengths at each point in space when prescribed with the three parameters that it depends on mentioned above. (Landgraf and Crutzen, (1998))

JVAL uses the two-stream method of Zdunkowski et al, (1980) when solving the radiative transfer equation and applying Mie theory for calculating σ_i in the atmosphere. Essentially, this means that scattering by air molecules, aerosols and clouds are considered in two distinct directions (contributing to upward and downward irradiances). However, according to Wild et al, (2000) large aerosols and cloud droplets have a strongly forward peaked scattering phase function (scattering occurs strongly in the forward direction as described in section 3.4) which is not well represented using the two-stream approach. As such, Landgraf and Crutzen, (1998) demonstrates errors in the order of 10-20% in J value calculations in the presence of clouds and aerosols as a result of using the two-stream method. This is a factor to be noted when attempting to diagnose differences between J value data from GEOSCCM and MESSy.

4.3 - Fast-JX

Fast-JX is the name of the photolysis scheme used in GEOSCCM. It is the third iteration of the original photolysis scheme proposed by Wild et al, (2000) which was originally developed for tropospheric photochemistry. Fast JX builds on the previous two schemes (Fast-J and Fast-J2) by providing a full scattering radiative transfer calculation for 18 wavelength bins as well as updated treatment of optically thick clouds.

Fast-J employed the use of 7 wavelength bands spanning the visible and near-UV spectral region used for photolysis calculations pertaining to tropospheric photochemistry. The exact resolution of these wavelength bins are shown in Table 2. The bin spacing for the wavelength bands appear to be arbitrary upon initial inspection, however they were chosen in order to minimize relative root-mean-square errors (to within 3%) between known J values of O_3 (to $O(^1D)$), NO_2, HNO_3 and H_2O_2 to those calculated over a range of atmospheric conditions (e.g. Clear sky, clouds, solar zenith angles) (Wild et al, 2000).

Band	Name	λ_{Ini} (nm)	λ_{fin} (nm)
1	Schumann-Runge	178.6	202.0
2	Hertzberg	202.0	241.0
3	Hartley	241.0	289.9
4		289.9	305.5
5	UV-B	305.5	313.5
6		313.5	337.5
7	UV-A	337.5	422.5
8	Chappuis	422.5	682.5

Table 1 - Spectral wavelength bands used In J value calculations in JVAL (Sander et al, 2014)

Band	λ_{Ini} (nm)	λ_{fin} (nm)
1	289.00	298.25
2	298.25	307.45
3	307.45	312.45
4	312.45	320.30
5	320.30	345.00
6	345.00	412.45
7	412.45	850.00

Table 2 - Spectral wavelength bands used in Fast-J for tropospheric photochemistry (Wild et al, 2000)

An extra 11 wavelength bins are added in the second iteration of the photolysis scheme, Fast J2, between 117-290 nm in order to extend the scheme into the stratosphere and lower mesosphere (Bian and Prather, 2002). This means that both models include wavelength ranges pertaining to all of the photolysis reactions that are relevant to this project (reactions (3.1) – (3.4) as well as stratospheric O_2 photolysis). Fast-JX builds upon the previous iteration by updating solar flux and cross-section datasets used in photolysis calculations as well as providing a more rigorous treatment of optically thick and overlapping clouds which will be discussed later.

Fast-J (and thus Fast-JX) does not employ the two-stream approximation when solving radiative transfer. Instead it solves an 8-stream multiple scattering problem using the exact scattering phase function, where the specific intensity (pertaining to actinic flux in photolysis calculations) is calculated for scattered light in 8 directions (4 upward and 4 downward) and integrated over all solid angles to obtain a mean intensity (Wild et al, 2000). The main advantage of this is that, similar to how wavelength bins were optimised to reduce relative errors compared to known J values, this 8-stream method was numerically developed to optimise the scattering phase function for large particles such that the errors introduced by the two-stream method due to aerosols and clouds are no longer present.

4.4 - Fast-JX and JVAL – key differences.

To summarise, JVAL and Fast-JX are two separate photolysis schemes employed by MESSy and GEOSCCM respectively to calculate photolysis rate coefficients for all of the shortwave photolysis reactions that occur in the troposphere and the stratosphere. Radiative transfer is solved by taking into account scattering due to a range of particles and provides actinic flux values in space and time which subsequently allows calculation of J values.

Fast-JX has two main advantages, namely the optimization of the scattering phase function expansion as well as optimization of integration over wavelength bins (Voulgarakis et al, 2009; Wild 2000). As mentioned previously, the two-stream delta-scaling method as described in

Landgraf and Crutzen, (1998) is known to introduce some significant uncertainties in the presence of large scattering particles such as cloud droplets and aerosols. This is a reduction of the full scattering problem along with the use of the σ_i parameter which is also an abstraction to encapsulate scattering which Fast-JX aims to do via truncation of the full scattering phase function. (Wild et al, 2000).

As a result of this. It is proposed that Fast-JX possesses a more sophisticated treatment of scattering and wavelength binning compared to JVAL, and there is a possibility that this can manifest itself as a more accurate representation of global distribution of $J(NO_2)$ and $J(O^1D)$ values. The former also incorporates an updated treatment of optically thick and overlapping cloud layers into photolysis calculations which is discussed further.

4.5 - Cloud implementation and overlap methods

The amount of cloudiness present in the atmosphere in a CCM has to be quantified by an amount associated with each grid-box as a result of how space is defined in the model itself. Cloud cover in a model level is usually prescribed as the amount of water in liquid/ice phase (cloud water content) and the fractional area occupied by a cloud (CF, from 0 to 100% of each grid-box) (Neu et al, 2007). Clouds can arrange themselves in a vast array of different vertical orientations, some of which consists of several overlapping layers of cloud decks. When represented in CCMs, this will alter the cloud optical depth τ of the entire column of cloudy grid-boxes which affects solving of radiative transfer.

Despite the many different vertical orientation of clouds, there are a few patterns that are representative of the many vertical cloud profiles found in the troposphere. For example tropical deep convective clouds could span the entire vertical extent of the troposphere with cirrus clouds overlying these and extending across to adjacent clear-sky regions (IPCC 5th report; Neu et al, 2007). A summary of oceanic vertical cloud profiles that exist in the troposphere can be seen in figure 2.

There are three main methods that CCMs use to take into account overlapping of clouds, they consist of the linear assumption (LIN) which involves spreading clouds uniformly over an entire grid-square with optical depths reduced such that $\tau' = \tau \times CF$ is the new optical depth, the random overlap method (RAN) which assumes that clouds in adjacent vertical layers have no correlation and the maximum-random overlap method (MRAN) which assumes that adjacent groups that are expected to be connected are maximally overlapped with the groups themselves randomly overlapping. All three methods have been extensively evaluated in the past (Liu et al, 2006; Feng et al, 2004) with Feng et al, (2004) finding that RAN and LIN underestimates and overestimates both $J(O^1D)$ and $J(NO_2)$ significantly in the lower troposphere and upper tropical troposphere respectively.

Both GEOSCCM and MESSy uses MRAN, however they are implemented differently in their respective models. The two different implementations of the same cloud overlap scheme is a result of the separate photolysis schemes that are used and thus their methods of implementation must be different according to how radiative transfer is solved as described in section (4.4). Any biases as a result of MRAN found by Feng et al, (2004) or any other evaluations of MRAN won't necessarily apply to these two CCMs unless they are implemented under the same photolysis scheme.

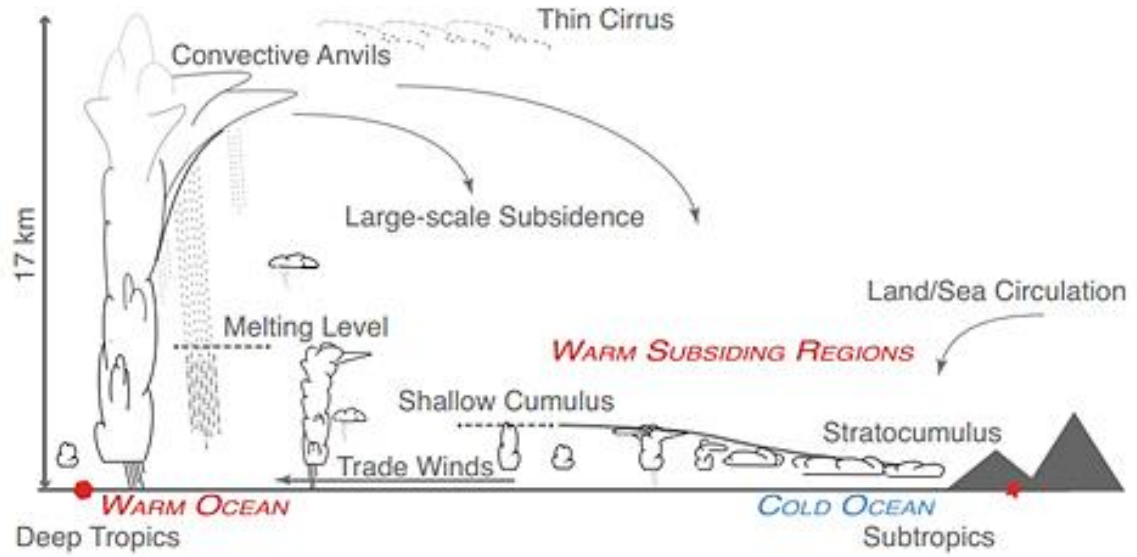

Figure 2 - Prominent vertical cloud profiles found in the oceanic troposphere (IPCC 5th assessment report, 2003). Warm oceans in the tropics give rise to deep convective cumulus clouds with overlying optically thin cirrus clouds whereas cold oceanic regions produces shallow convective stratocumulus clouds. Convective clouds subside high up as they reach the tropopause due to the change in lapse rate producing more buoyant air above.

4.6 – Maximum-random cloud overlap scheme

As mentioned previously, implementations will be different depending on the model and understanding the differences between the two implementations of MRAN in MESSy and GEOSCCM is crucial for diagnosing any biases in cloud cover in the models relative to observations as well as differences in enhancements/reductions of J values as a result of clouds between models. According to references cited by Neu et al, (2007), MRAN has been shown to be a reasonable representation of observed cloud distributions over several regions including the midlatitude and tropical oceans, central England as well as midlatitude continental sites.

In its simplest form, the MRAN scheme involves splitting a given vertical profile of cloud fraction into several different configurations. Each vertical layer of each configuration is either fully covered (CF=100%) or clear (CF=0%). It is assumed that photochemistry for the entire vertical profile can be treated linearly such that integrations over all the different configurations is representative of such a profile. Additional layers of complexity are then added by considering the weighting and grouping of such configurations. An illustration of splitting of a vertical profile of clouds into its configurations is shown in figure 3.

Fast-JX implementation of MRAN involves a quadrature approximation of integration over a selection of configurations to reduce computation times whereas JVAL modifies its σ_i parameter according to alterations of cloud optical depth τ as a result of MRAN cloud overlaps (Neu et al, 2007, Roeckner et al, 2003). A full theoretical analysis of the differences between the two implementations would be ideal, however the scope of this project involves working backwards i.e. tracing the differences in J values back to the differences in implementation of MRAN as well as photolysis schemes.

4.7 - Model summary

Table 3 is a summary of the main relevant specifications of the two CCMs that are examined in this project. GEOSCCM has a slightly higher spatial resolution relative to MESSy which in turn includes an extra year for some of the variables examined (for the sake of consistency intermodel comparisons will use data spanning the same number of years). To summarise, differences between models in the results discussed later should be diagnosed by analysing the differences between the two models shown in table 3, namely the separate photolysis schemes, scattering treatment and cloud-overlap implementations. This paves the way for potential future analysis on evaluations of photolysis and cloud treatment that may not be discussed in this project.

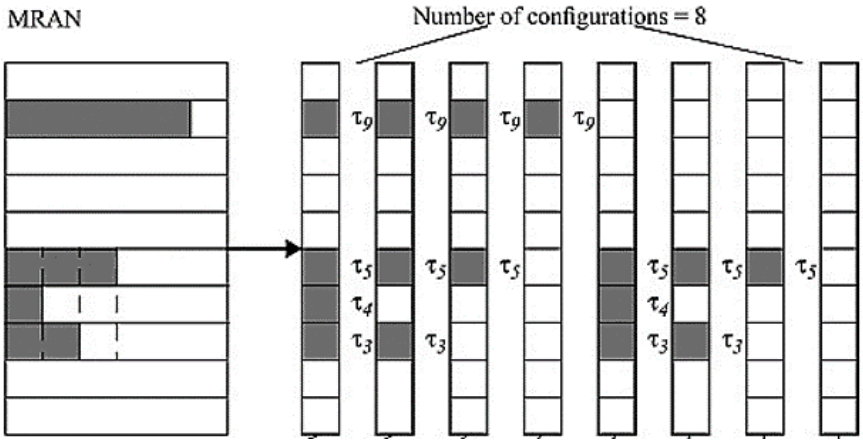

Figure 3 – Schematic of the MRAN overlap scheme for a simplified 10-level vertical cloud profile. 8 configurations are produced using the scheme prescribed by Feng et al, (2004). The in-cloud optical depths at vertical layer i is equal to τ_i

	GEOSCCM	**MESSy**	**References ([GEOSCCM]/[MESSy])**
Full name	Goddard Earth Observing System – Chemistry-Climate model	ECHAM/MESSy Atmospheric Chemistry model	[Oman, L. D., and A. R. Douglass (2014)]/[Stevens et al, (2013)]
3D resolution (Lon/Lat/Lev)	144/91/(72/41)*	128/64/47	
Temporal resolution	Monthly (1960-2010)	Monthly (1960-2010/2011)	
Cloud-overlap method	Maximum-random	Maximum-random	[Neu et al, (2007)] / [Roeckner et al, (2003)].
Photolysis scheme	Fast-JX	JVAL	[Wild et al, (2000), Bian and Prather, 2002, Neu et al, (2007)] / [Landgraf and Crutzen, (1998), Sander et al, (2014)]
Interactive photolysis	Online	Online	
Scattering treatment	8-stream full scattering	2-stream delta scaled	[Wild et al, (2000)] / [Landgraf and Crutzen, (1998)]

*Table 3 – Relevant specifications of the two analysed CCMs along with accompanying references. *due to availability of data, $J(O^1D)$ and $J(NO_2)$ were provided at a reduced vertical resolution.*

5. Methodology

Data outputs from models participating in CCMI are uploaded to the British Atmospheric Data Centre (BADC) and was downloaded from the website

(http://browse.ceda.ac.uk/browse/badc/wcrp-ccmi/data)

Downloaded monthly variable data for GEOSCCM and MESSy are in the form of 3D/4D-arrays with an assigned value for each point in space (longitude/latitude/level) and time corresponding to spatial and temporal coordinates of the grid-boxes. Spatial dimensions vary in units of grid-box location whereas the temporal dimension varies monthly spanning 1960-2010. Table 4 shows a list of the main variables that were used for this project.

5.1 – Correlation analysis

The main analysis that was carried out consisted of looking at associations between variables, particularly between cloud fraction (2D and 3D) and photolysis rates/mixing ratios. To do this linear pearson correlation coefficients were calculated for the two variables, specifically correlations between annual mean values of the two variables. This means that calculated correlations are a result of interannual variability or long term trends between annual mean data. Therefore the raw monthly variable data needs to be averaged yearly in order for correlations to be calculated. Calculating annual means for monthly variable data has two key benefits, firstly the seasonal cycle is removed such that correlations between the two variables will not be a result of known seasonal effects of increasing and decreasing solar intensity in summer and winter hemispheres respectively, as well as known regional varying cloud climatology. Secondly annual means allow for a clear representation of trends in variable data such that any prominent annual scale long term trend and potentially its cause (if affected by an equal long term trend in another variable) can be shown using line plots (see figure 5). Annual means span 50 years according to availability of data therefore each variable will have 50 annual mean values.

Variable name	Description	Spatial dimensions	Units
clt	Total cloud fraction - the percentage area of each gridbox that is covered by cloud for the entire atmospheric column, viewed from TOA or the surface.	2D	%
cl	Cloud area fraction - A 3D cloud fraction quantity assigning grid boxes in each CCM layer with the fractional area covered by clouds	3D	%
vmroh	Molar volume mixing ratio of OH in air	3D	1
vmrh2o	Molar volume mixing ratio of H_2O (in vapour form) in air	3D	1
jno2	Photolysis rate of NO_2	3D	s^{-1}
photo1d	Photolysis rate of O_3 to O^1D	3D	s^{-1}
clw	Mass fraction of cloud liquid water content in air	2D	1
areacella	Area spanned by each grid-box	2D	m^2
airmass	Vertically integrated mass content of air in layer	3D	Kg m^{-2}

Table 4 – Variable descriptions for data used.

5.2 - Weighting

Averages were calculated in several ways depending on the type of plot that was produced. For regional correlation bar plots (see figure 8), the variable was averaged spatially such that each month is assigned an average value for a given region. Regional monthly averages are then used to calculate an ordinary arithmetic annual mean assigning equal weighting to each month. Because of spherical geometry, each grid-box is not of equal area. Grid-boxes near the equator are larger in area compared to those near the poles (this is represented in figure 4 using the areacella variable). Therefore it is appropriate to assign more weight to values of 2D variables (such as clt) in grid-boxes near the equator. To do this a weighted mean is calculated when spatially averaging such that the regional monthly average for a 2D variable (clt in this example) is calculated using equation (5.1)

$$\overline{clt(t)} = \frac{\sum_{i,j} clt_t(\lambda_i, \varphi_j) \times A(\lambda_i, \varphi_j)}{\sum_{i,j} A(\lambda_i, \varphi_j)} \quad (5.1)$$

where $\overline{clt(t)}$ is the average clt value for month t, λ_i and φ_j are longitude and latitude coordinates respectively (subscripts i,j are used to denote a sum over a specific selected region) and A is the area of the grid-box at location (λ_i ,φ_j). For 3D variables more weight is instead given to grid-boxes with a larger air mass. In this case, equation (5.1) is extended to sum over all i,j,k where 3D variables such as $jno2 = jno2(\lambda_i, \varphi_j, l_k)$ where l_k denotes the height coordinate, and A is replaced by the airmass variable $M(\lambda_i, \varphi_j, l_k)$. For annual mean maps (see figure 7) specific regions are not defined, therefore annual mean values are calculated for each grid-box and thus weighting is not required for 2D variables, however 3D variables are still weighted vertically by air mass.

5.3 - Detrending

Removing prominent long term trends from annual mean data implies that correlations between variables are now solely due to interannual variability. To do this, a linear fit was applied to annual means and was removed by subtraction. This method is able to account for any monotonous trend in annual mean data, as illustrated in figure 5. However for long term trends that aren't monotonous, detrending with this method will not remove the trend entirely. If this was seen to be the case (e.g. from observing line plots), a running average was calculated to represent the trend (rather than applying a linear fit) and subtracted in order to remove the non-monotonous trend. (N.B. this was not used extensively in this project as non-monotonous trends were rarely encountered, notably only for J(O^1D) correlations).

5.4 - ISCCP observational data

In order to validate simulated cloud climatology, model cloud data was compared with observational data obtained from the D2 dataset of the International Satellite Cloud Climatology Project (ISCCP) which was downloaded from the ISCCP website (http://isccp.giss.nasa.gov/products/browsed2.html). ISCCP was established in 1982 to collect and analyse satellite radiance measurements to infer global distributions of clouds as well as their properties and variations. Description and details of cloud-detection algorithms from ISCCP observational satellites are given by Rossow and Schiffer, (1999). A map of global total cloud amount was downloaded to compare with cloud climatology maps produced for MESSy and GEOSCCM using the clt variable. ISCCP observational data contains instrumental uncertainty which is significant mostly in the poles (Rossow and Schiffer, 1999).

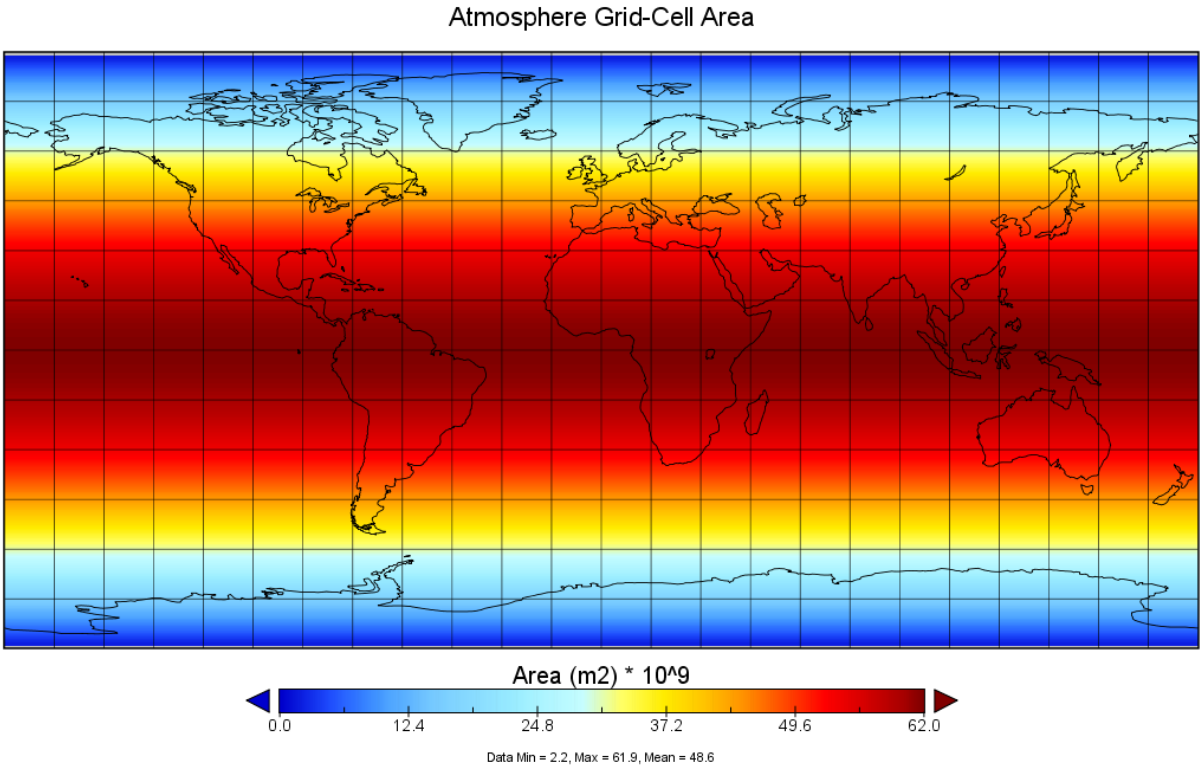

Figure 4 – Spatial spherical geometry of grid-boxes in GEOSCCM showing larger grid-box area near the equator. Grid lines in this figure do not correspond to the locations of the grid-boxes. Grid-boxes are at a higher resolution as seen by the fine colour scale variations.

5.5 - Region definition

Regions were defined to cover locations with a variety of different vertical cloud profiles over both land masses and oceans (See Appendix A for the region locations and exact region definitions). South-eastern regions of the Pacific and Atlantic oceans were selected as they are known to be regions of persistent and spatially extensive high fractional stratocumulus cloud coverage due to the cool waters below. The southern midlatitude oceans were selected because observations of cloud climatology showed the regions to contain high total cloud fractions. Sections of the Atlantic and Pacific were looked at individually to observe the effects of several oceanic vertical cloud profiles on photolysis. Several high latitude, tropical and sub-tropical land mass regions were selected in order to observe cloud and photolysis over a variety of different continental climates.

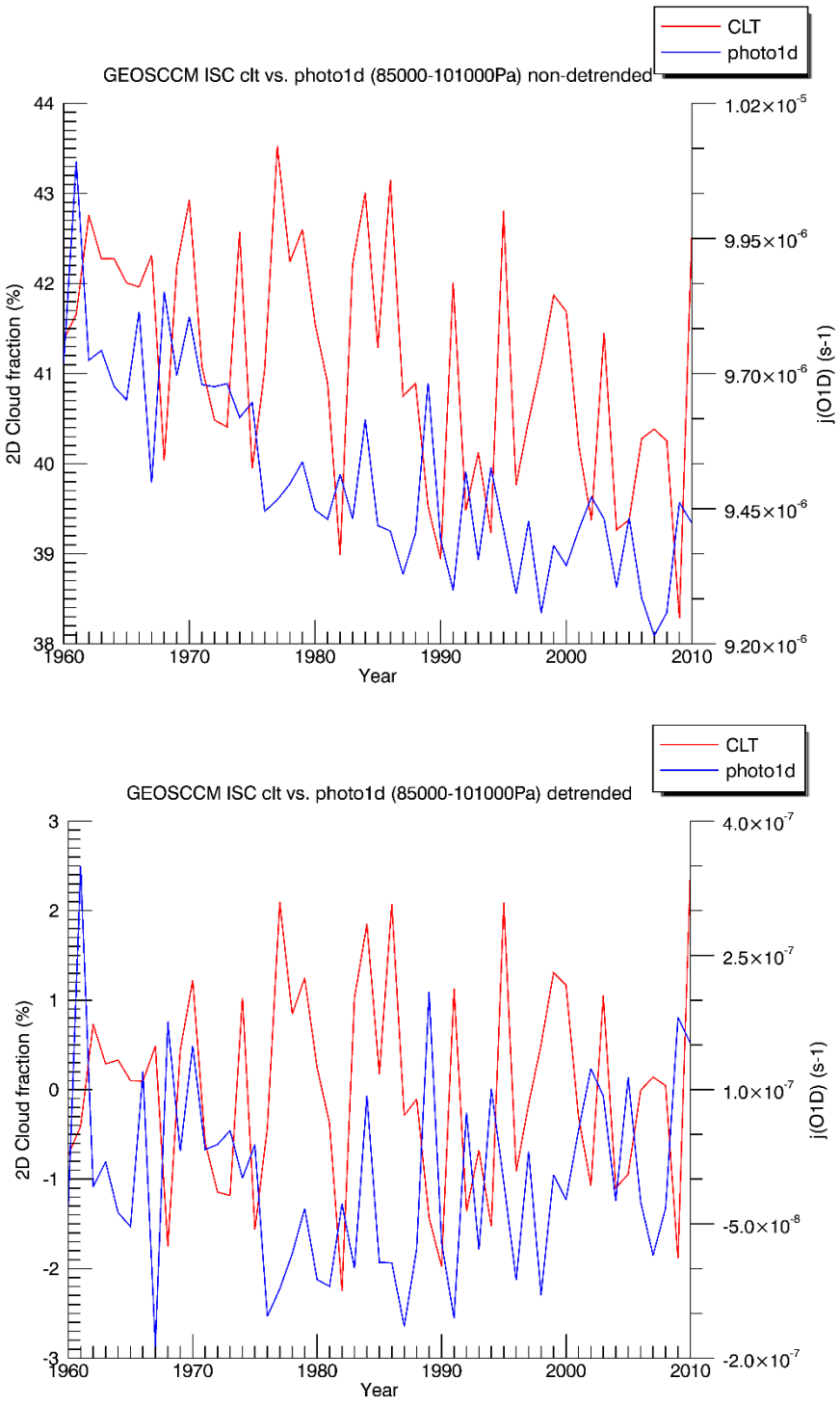

Figure 5 – *Regional (ISC) line plots to illustrate the detrending method. J(O^1D) and clt before detrending (top) and after detrending (bottom) showing the removal of the monotonous trend in both variables whilst keeping the interannual variability, allowing correlations to be calculated in the absence of long-term trends.*

6. Results

6.1 – Cloud climatology

Monthly total cloud fraction was averaged over a 27 year period using the clt variable to produce maps of global cloud climatology and was compared with ISCCP observations (see figure 6). Excluding the poles (which are known to have biases and are not well represented in ISCCP) GEOSCCM stands out, having a striking systematic bias in total cloud fraction compared to observation with biases on the order of approximately -20% in most regions and up to -50% in the south-eastern Pacific and Atlantic. Cloud climatology in MESSy is more similar to ISCCP whilst both models have similar distributions of cloud cover compared to observation when neglecting the actual values. It is known that uncertainties in ISCCP D2 cloud cover away from the poles is approximately 10% resulting from errors in clear-sky radiances. This means that clouds are mostly well represented in MESSy, whereas GEOSCCM as mentioned before has a significant global low bias in cloud fraction.

It is not immediately obvious why this is the case for GEOSCCM. Total cloud fractions affect MRAN implementation and not vice versa so it is unlikely that the bias is due to a poor representation of cloud overlap. Luke Oman (personal communication, 2016) confirmed that this bias has been seen before from previous cloud evaluations and states that cloud climatology has a better agreement with observation when higher spatial resolutions are used, which isn't surprising as higher spatial resolutions results in better sub-grid cloud representations. Lower total cloud fractions implies less clouds in general and thus a lower concentration of optical depth altering properties in clouds. If this is the case, a cloud optical depth climatology comparison should show MESSy having higher cloud optical depth in persistently cloudy regions compared to GEOSCCM. Due to availability of data, these comparisons could not be made. Cloud water content (mass fraction of cloud water content in air) is a concentration quantity that directly affects cloud optical depths for certain photolysis reactions since an increase in concentration of cloud droplets (in both liquid and ice phases) results in increased scattering. Therefore a reduction in cloud liquid water content (and thus optical depth) is expected to accompany the low bias in cloud fraction seen in GEOSCCM (water content including ice would be a better variable to use, but this was not available).

6.2 - Cloud liquid water climatology

A model comparison of total column cloud liquid water content using the clw variable is shown in figure 7. In the figures shown, the scales are adjusted such that the maximum values that appear in the maps are the same, however the maximum values of clw for MESSy are actually approximately 4 times those of GEOSCCM and isn't represented in the colour scale (note the small writing underneath the scale). GEOSCCM possesses considerable amounts of cloud liquid water over the southern extratropical oceans which is consistent with the model's cloud climatology as this is one of the regions where biases in total cloud fraction is smallest. If a systematic global underestimate of clouds in GEOSCCM is believed to exist, then cloudiness in the model may be favoured in this southern oceanic region. Previous applications of Fast-JX with prescribed water contents found an overestimation of cloudiness in these regions corresponding to the position of persistent southern hemisphere marine stratus clouds (Voulgarakis et al, 2008). This overestimation of cloudiness is also present in evaluations of previous iterations of GEOSCCM's core general circulation model GEOS-3 (Liu et al, 2006) and it is likely that this may be the case even for the iteration used in the current model (namely GEOS-5).

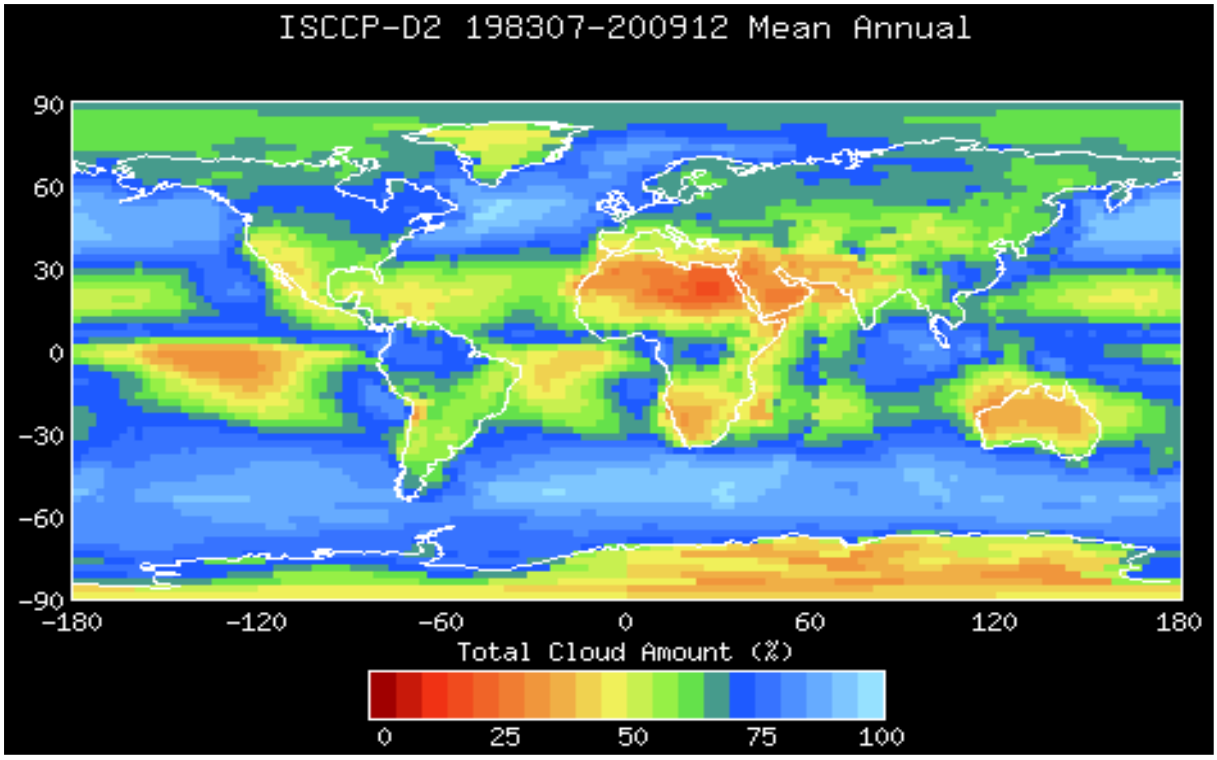
ISCCP-D2 198307-200912 Mean Annual
90
60
30
0
-30
-60
-90
-180
-120
-60
0
60
120
180
Total Cloud Amount (%)
0
25
50
75
100

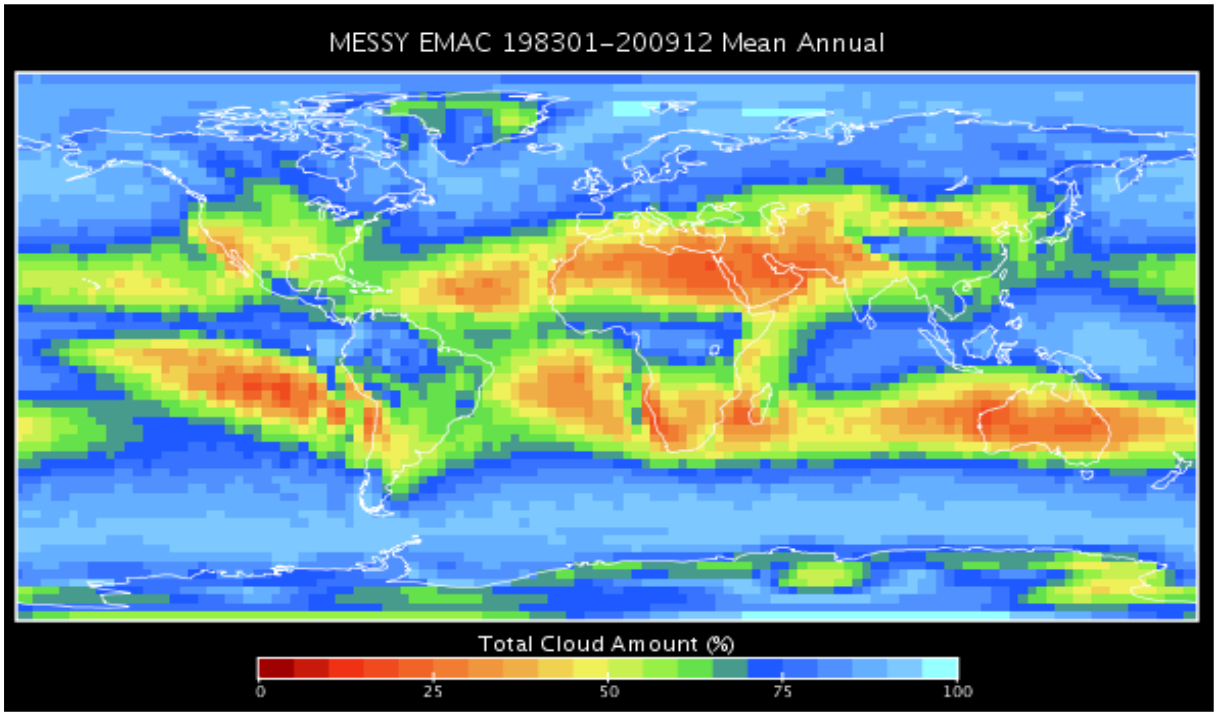
MESSY EMAC 198301-200912 Mean Annual
Total Cloud Amount (%)
0
25
50
75
100

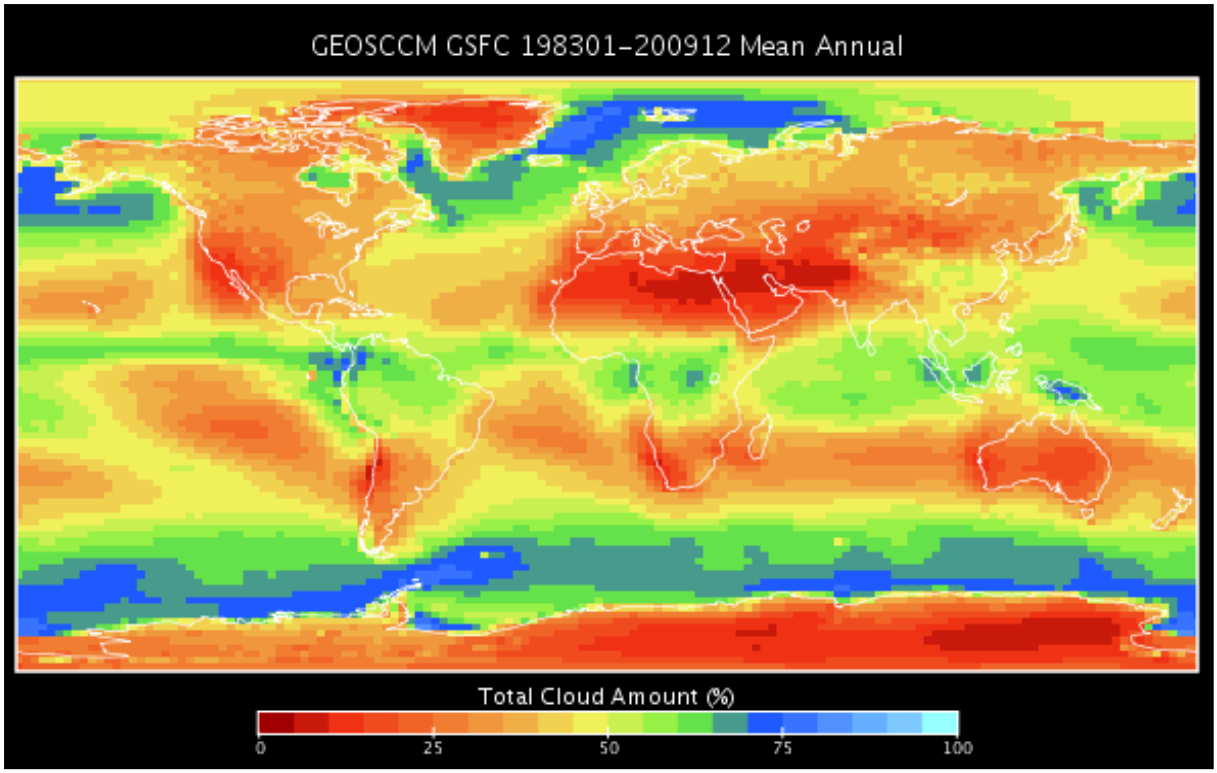

Figure 6 – Total cloud amount climatology spanning a 27 year period from ISCCP observational data compared to the simulated cloud climatology of MESSy and GEOSCCM, listed in the order they appear.

Excluding this region, cloud liquid water content seems to be significantly greater over several land mass regions in MESSy compared to GEOSCCM including over South America, Europe, South-East Asia and a few regions over Africa. This may be due to an increased presence of cloud condensation nuclei (CCN) on which liquid cloud droplets can form. These CCN's are likely to be aerosols over the Asia, Africa and South America regions (where biomass burning occurs) and sea salt particles over the ocean regions (North and East Pacific and North Atlantic). However it is not known known whether MESSy has overprescribed these CCN's or GEOSCCM is underestimating cloud water content in general, a comparison with actual values of cloud liquid water content from observation is required to confirm this. Overall it is difficult to infer using these maps whether cloud optical depths will be higher for MESSy compared to GEOSCCM. Whether the presence of increased cloud liquid water content over the land regions will affect photolysis rates or not will be investigated by examining cloud and photolysis correlations.

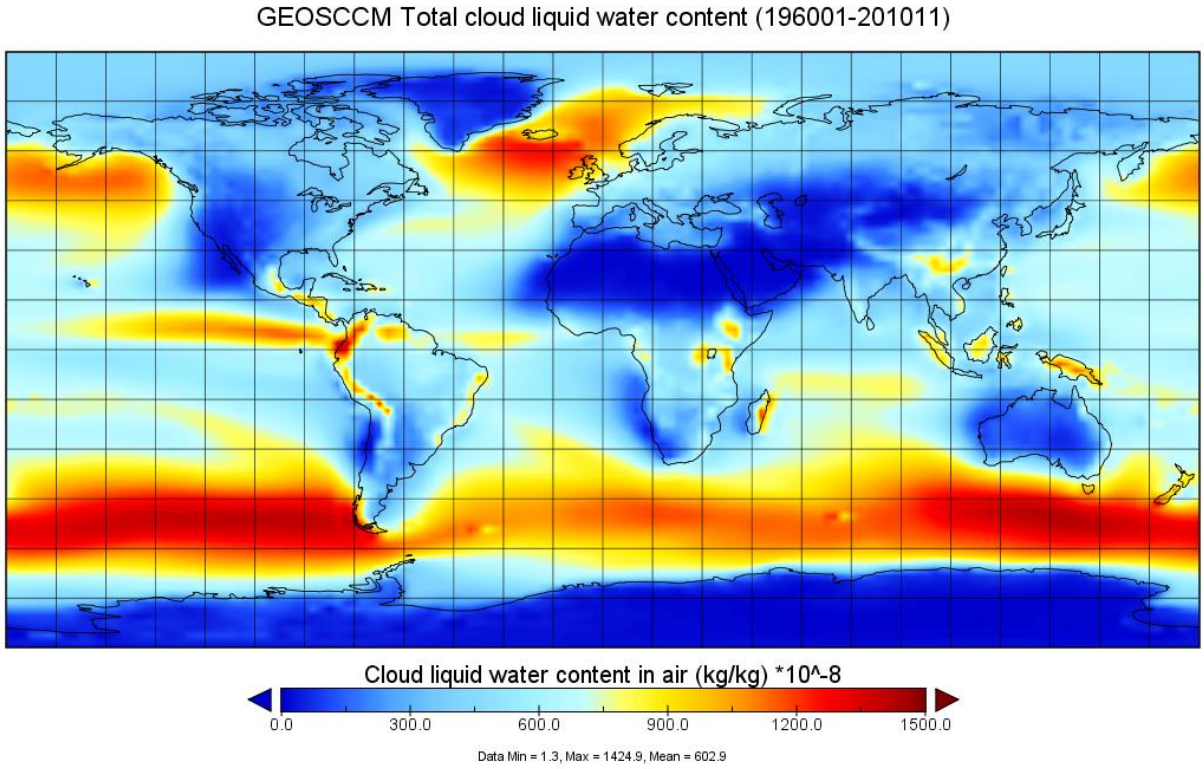

Figure 7 – Climatology of total column cloud liquid water content for GEOSCCM (top) and MESSy (bottom) produced using clw variable. Maximum values of clw for MESSy are lost to saturation of the scale which was adjusted to match that of GEOSCCM for comparisons to be made.

6.3 - J(NO_2) correlations

Due to the bias of cloudiness in GEOSCCM, it might be expected that correlations between photolysis rates and clouds will be affected by the implications of absence of clouds as mentioned previously, however without cloud optical depth climatology comparisons it is difficult to say whether this will be the case. Regardless, figure 8 shows correlations of annual mean total cloud fraction (clt) with annual mean photolysis rates of NO_2 (jno2) for several regions (see Appendix A for exact region definitions).

The most striking feature is actually the agreement of correlations between the two models which may indicate that low levels of cloudiness in GEOSCCM doesn't affect the scattering properties (thus optical depth) of clouds in the model. Two regions coinciding with the high levels of cloud liquid water content found in MESSy are SAM and ISC (South America and the Indian Subcontinent respectively). The correlations for these regions are for the most part very similar, with the differences in correlations mainly existing in the adjacent altitude bands where correlation transitions between negative and positive occur, as result of the transitions between attenuation and enhancement of radiation due to clouds respectively. It is likely that these differences are a result of disagreement between models of the height where the bulk of cloud water content exists, which is roughly where transitions between enhancement and reduction of photolysis rates occur. (Voulgarakis et al, 2011)

The similarities in the magnitude of correlations between the two models may suggest that the bias in total cloud fraction doesn't affect cloud optical depth for J(NO_2) in GEOSCCM. This is somewhat consistent with information supplied by Luke Oman, (personal communication, 2016) implying that the bias may be due to a deficiency in cloud representation using cloud fraction variables in GEOSCCM. It could also be due to an overestimation in global J(NO_2) values as a result of a deficiency in calculation of photolysis rates of NO using Fast-JX. Telford et al, (2013) found this to be the case for previous iterations of the photolysis scheme under idealised conditions, showing a significant global positive bias in J(NO_2) throughout the atmosphere. However from inspection, the magnitude of J(NO_2) values between models is in agreement (in the same order of magnitude at the boundary layer and at TOA) so it is likely that low biases in total cloud fraction are a result of misrepresentation of clouds.

To check if the 3D cloud variable (cl) also contains this bias, vertical cloud profiles using the variable was created over the several regions. The profiles showed that the low bias persists even in the 3D cloud fraction variable for GEOSCCM throughout the entire vertical extent of the atmosphere for nearly all regions, although cloud profiles of continental regions with low cloudiness such as Austrailia (AUS) are in agreement due to the regional absence of clouds themselves rather than an agreement of the representation of clouds. See Appendix B for cloud profiles (made using the 'cl' variable) over these regions.

Correlations are different as expected over oceanic regions where different vertical cloud profiles exist. Over the cool waters of the South-eastern Pacific and Atlantic (SEP, SEA), shallow convection persists and the vertical extent of clouds are not very high, leading to an overall positive correlation throughout the atmosphere due to lack of attenuation, only slightly reducing at lower altitudes where the extent of clouds are. The central Pacific is a region of persistent deep and shallow convection due to the warm waters and climate, therefore cloud water content actually peaks at two points in the atmosphere (Voulgarakis et al, 2011) and photolysis rates are modified similar to the schematic in figure 1 in section (3.4) causing a net correlation profile similar to those over continental regions.

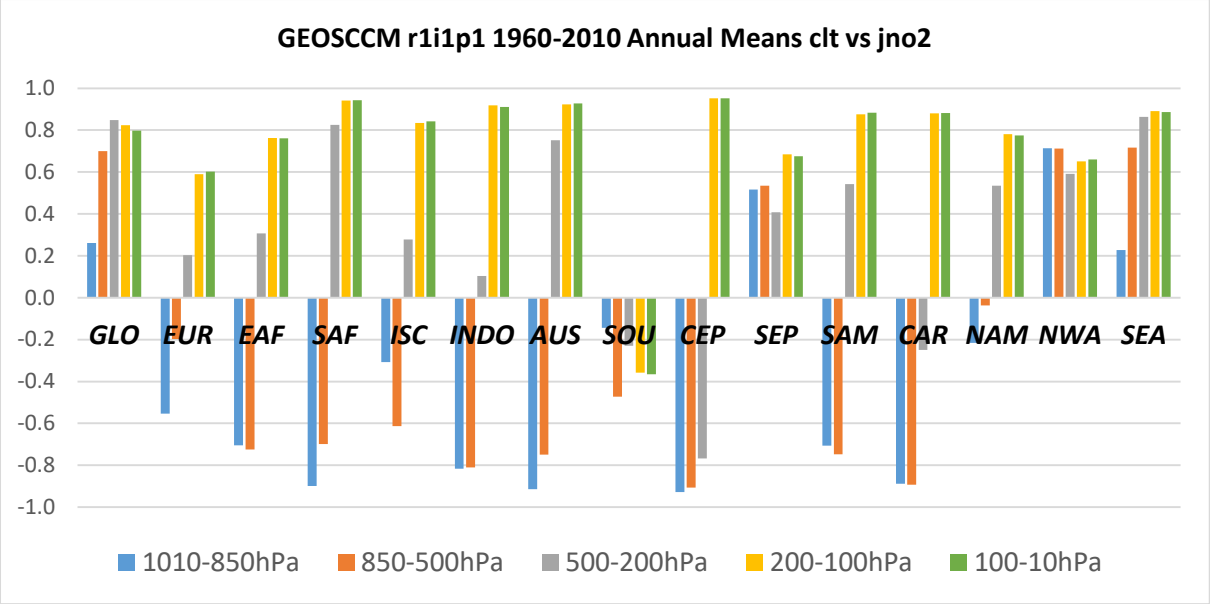

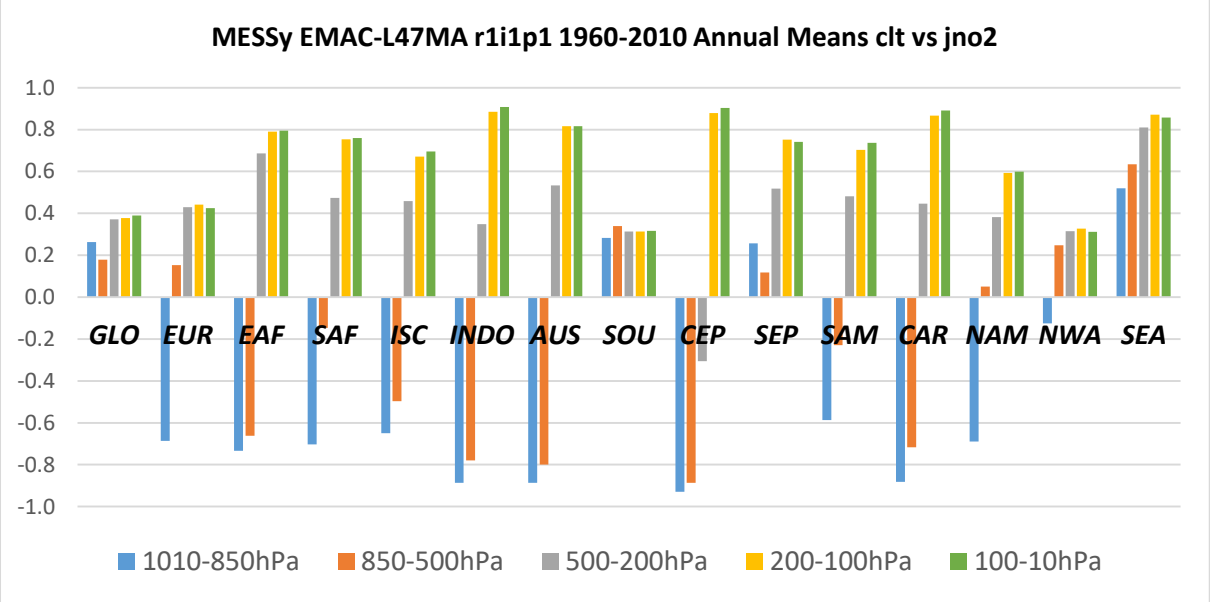

Figure 8 – Annual mean correlations for GEOSCCM (top) and MESSy (bottom) between J(NO_2) and total cloud fraction for several altitude bands across all the regions studied.

Over the southern oceans (SOU), there is disagreement between the two models, with negative correlations throughout the atmosphere for GEOSCCM compared to a positive correlation throughout for MESSy. This is likely due to the biases in cloudiness in GEOSCCM mentioned previously affecting correlations. Vertical cloud profiles over the Northwest-Atlantic (NWA) are similar to those found in the Southern oceans and so it is expected that correlation profiles should be similar for these two regions (the case for MESSy), with the difference at low altitudes in NWA likely due to capturing of subsidence along the edges of continental regions.

Lack of a meaningful negative correlation low down for North America (NAM) in GEOSCCM is due to the small levels of cloudiness over this extratropical continental region not attenuating and thus producing a strong negative correlation. Globally both models agree on a persistent positive correlation throughout the atmosphere, although averaging over the many cloud profiles and climates doesn't provide too much useful insight. Annual mean detrended correlations between clt and jno2 were also produced, however these results were omitted as bar plot correlations turned out virtually the same indicating a lack of any long-term trend prominent enough to affect expected correlations.

6.4 - J(O^1D) correlations

Figure 9 shows correlations of annual mean total cloud fraction (clt) with annual mean photolysis rates of O_3 to O^1D (photo1d). Correlations are overall lower in magnitude compared to correlations of clouds with J(NO_2) as expected since J(O^1D) depends on several other factors which may overall reduce the dependence on the radiative properties of clouds. Focussing on correlations in MESSy, we can see over several regions that positive correlations begin to reduce considerably as you ascend the troposphere into the stratosphere with a maximum varying regionally between the pressures bands of 100hPa-500hPa. This reduction in correlations could be due to several reasons. Firstly, temperature drops with increasing altitude which begins decreasing the quantum yield of J(O^1D) reactions and thus starts affecting correlations high up. Scattering by clouds become diffuse away from cloud tops and this effect could be magnified higher up as other factors begin to dominate. Cloud water content also drops considerably close to the tropopause which further contributes to the previous effect. It is also likely that long-term trends are present higher up in the atmosphere that begins dominating, therefore reducing the dependence of J(O^1D) on clouds. This is likely to be the case for the difficult to explain annual mean correlations for GEOSCCM.

Figure 10 shows the same correlations after removal of long term trends using a linear fit. Still focussing on MESSy, we can see that higher up the positive correlations are now enhanced compared to the annual mean correlations, confirming that long term trends were beginning to dominate at the highest altitudes. For GEOSCCM, detrending results in significant differences between these correlations compared to annual means. It is likely that GEOSCCM is capturing long-term trends throughout the atmosphere that MESSy is omitting. Overall the radiative effects of clouds play much less of a role for J(O^1D) compared to J(NO_2) manifesting itself as smaller magnitudes of correlations in the detrended plots, otherwise the correlation profiles are similar to those of J(NO_2). To further explain the features seen, trend analysis is required which is done using line plots for the ISC (Indian subcontinent) region.

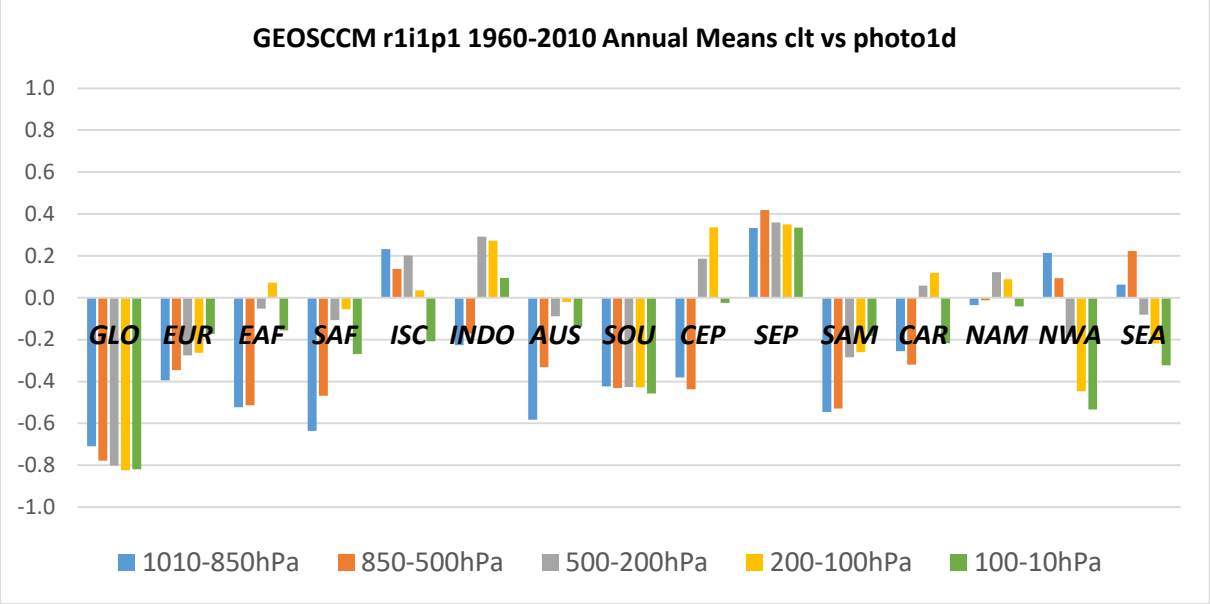

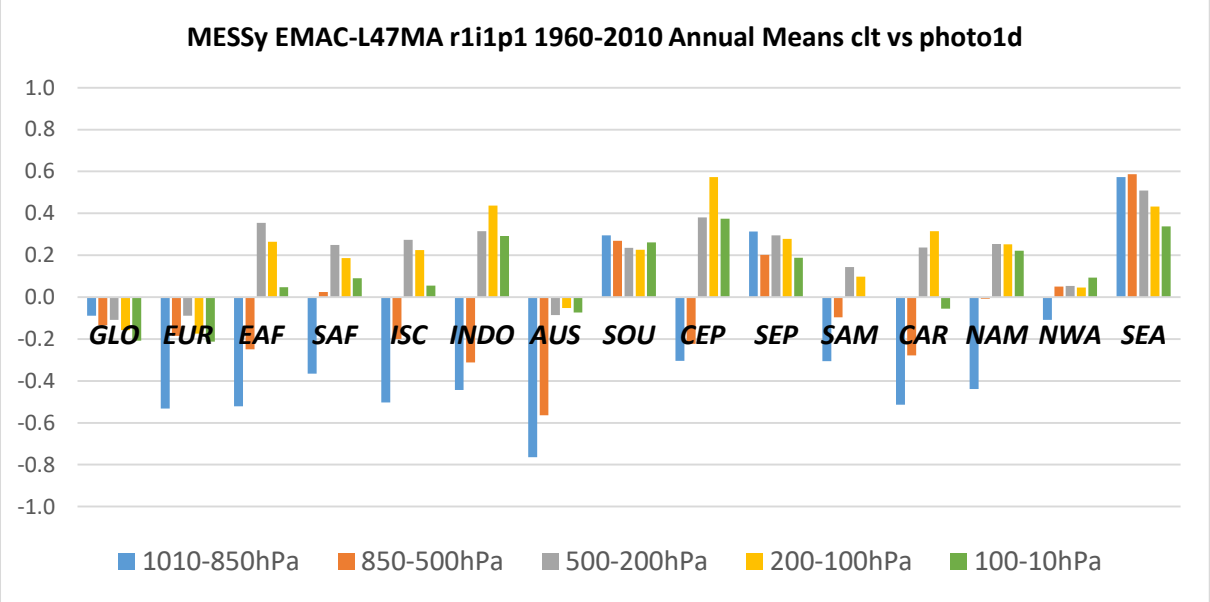

Figure 9 – Annual mean correlations for GEOSCCM (top) and MESSy (bottom) between J(O^1D) and total cloud fraction for the same altitude bands across all the regions studied.

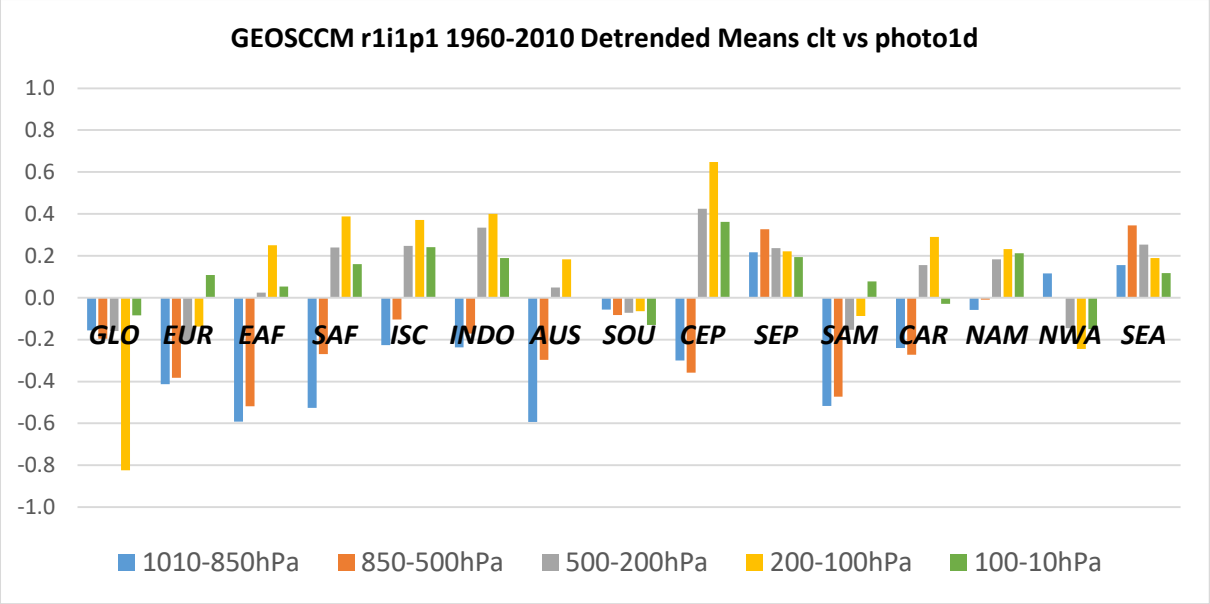

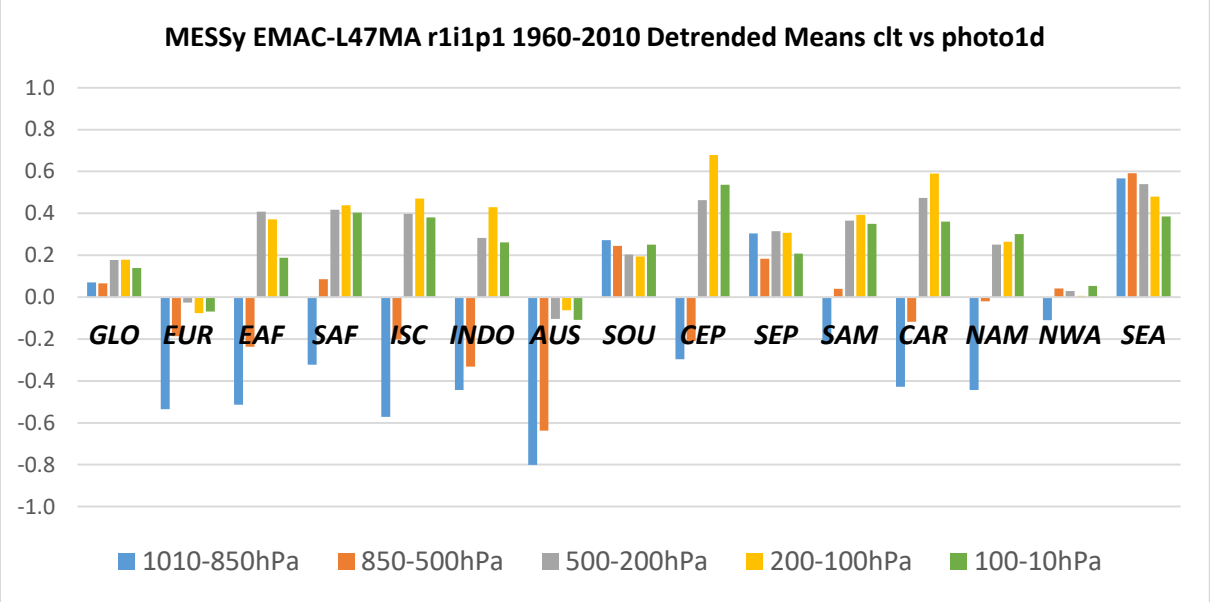

Figure 10 – Detrended annual mean correlations for GEOSCCM (top) and MESSy (bottom) between J(O^1D) and total cloud fraction for the same altitude bands across all the regions studied.

6.5 - J(O^1D) & Long term trends

An example of a long-term trend which may be affecting correlations between clouds and J(O^1D) in GEOSCCM can be seen from the line plot back in figure 5. The top panel line plot shows the interannual variability for clt and j(O^1D) for the ISC region at the lowest altitude band (boundary layer) without removal of long-term trends. We can see that there is a decreasing trend in both variables with a considerable surface layer dimming of J(O^1D). Determining the causes of such long-term trends is difficult and narrowing down the cause would require conduction of sensitivity analysis, for example observing the effect that removing a certain chemical species would have on J(O^1D) rates.

It is proposed that surface layer dimming of J(O^1D) could be due to a long term increase in overhead ozone column above the boundary layer altitude band considered. This proposition is derived from the fact that there is a feedback process involved with J(O^1D) where a reduction in J(O^1D) results in decreased loss of O_3 through photolysis. Vertical transport associated with convection could then bring O_3 to upper layers of the atmosphere, further reducing J(O^1D) below due to overhead absorption. To investigate this, J(O^1D) surface layer interannual variability (without detrending) is plotted with the overhead ozone mixing ratio for the ISC region which can be seen in figure 11.

In these line plots, you can see a increasing trend in overhead O_3 captured by GEOSCCM which is likely involved in the feedback of further reduction in surface layer J(O^1D), a feature that is not seen in MESSy. According to information provided, (Luke Oman, Patrick Joeckel, personal communication, 2016) JVAL does not take into account time-varying aerosol emissions when calculating photolysis rates which GEOSCCM does. Therefore, prescriptions of surface layer emissions of black carbon/sulphates which is known to be significant over regions of biomass burning (such as ISC) could be causing additional dimming of J(O^1D) due to absorption, which further contributes to the increasing trend in overhead ozone (specifically in the troposphere as we will see later on). If this is the case, it is a significant result as omitting time-varying aerosol information, specifically pertaining to its radiative properties, from a CCM could have drastic implications on tropospheric chemistry as a result of increased ozone production, which raises questions about the requirements for a CCM to actually claim the use of a fully interactive online photolysis scheme.

The advantage of plotting the interannual variability of ozone for the entire overhead column is it shows that the increasing trend of ozone is stronger than the trend of stratospheric ozone thinning which both models seem to agree on (figure 12). In the figure, interannual variability is plotted once again for surface layer J(O^1D) but here the ozone mixing ratio is for the altitude band of 10-100hPa, which includes a majority of the stratosphere above the tropopause. This shows that the increasing trend in ozone column is a tropospheric feature which compensates for the ozone thinning above, agreeing with the proposition that omitted aerosol properties causing dimming occurs in the troposphere and may be from emissions in the boundary layer. Stratospheric ozone thinning for ISC begins to level out towards the beginning of the 21st century as seen in figure 12, which implies it may be due to a reduction in prescription of ozone-depleting substances in the models. Previous evaluations of GEOSCCM show that there is a high-bias in high-latitude ozone which may affect several of the regions studied here, but it is not expected to affect the ISC region (Oman and Douglass, 2014). Note that thinning of stratospheric ozone does not affect boundary J(O^1D) in MESSy.

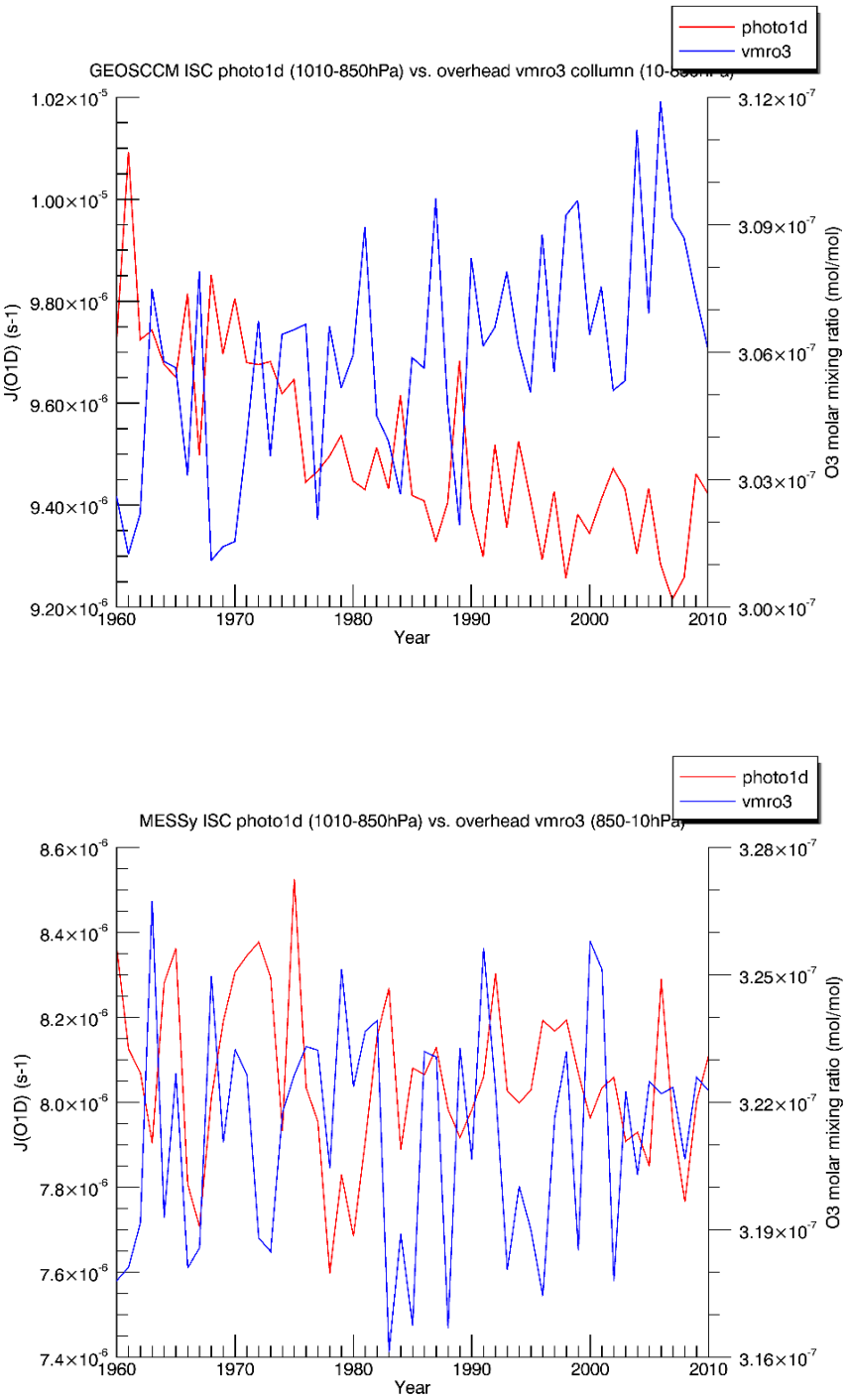

Figure 11 – *ISC interannual variability for boundary layer (1010-850hPa) J(O^1D) and overhead (850-10hPa) O_3 mixing ratio including the stratosphere for GEOSCCM (top) and MESSy (bottom).*

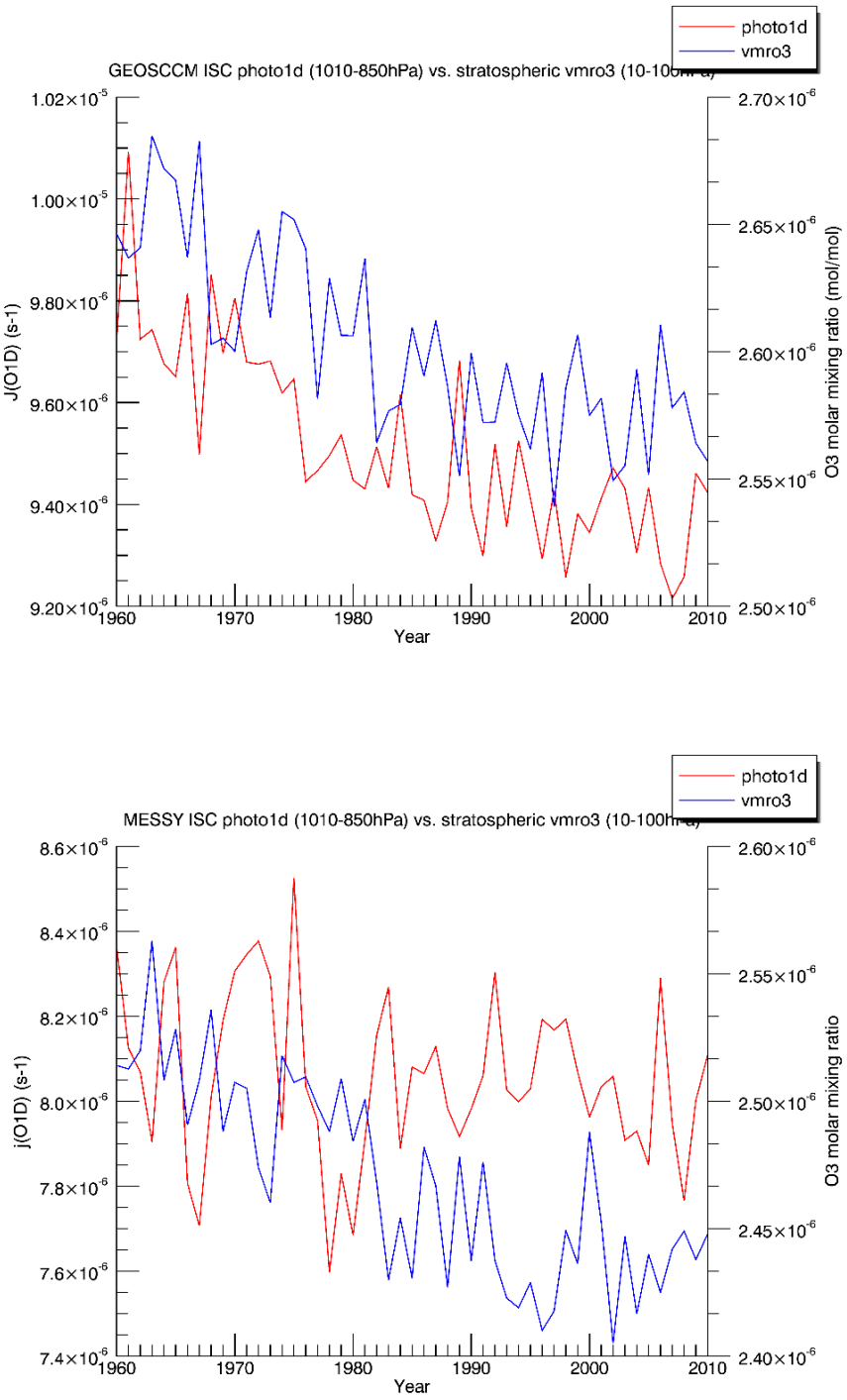

Figure 12 – *ISC interannual variability for boundary layer (1010-850hPa) J(O^1D) and stratospheric (10-100hPa) O_3 mixing ratio for GEOSCCM (top) and MESSy (bottom).*

Detailed trend analysis for other regions is subject for possible future work with the key information to take away being that deviations from the expected correlation profiles between clouds and $J(O^1D)$ is a clear indication that other factors are dominating the photolysis reaction (where detrending is a good tool to check this). However there are too many factors that affect $J(O^1D)$ reactions (many of which may not be accounted for in the models as seen previously) to draw an equal comparison and allow for evaluation of photolysis and clouds treatment. A better study would be to use known photolysis values of $J(O^1D)$ (perhaps from observational data) for specific regions and compare them to the modelled outputs seen here. In summary $J(O^1D)$ and cloud correlations should not be used for model setup evaluations.

6.6 – Cloud and OH correlations

It is expected that correlations between clouds and concentrations of OH should be strong as production of OH requires the combination of H_2O molecules with O^1D atoms produced by photolysis, where regions of high levels of cloudiness implies an abundance of these H_2O molecules. Given the bias in total cloud fraction, it would be interesting to see if there are significant differences between correlations of cloud and OH concentrations between models. Figures 13 and 14 show detrended annual mean correlations between total cloud fraction (clt) and OH molar mixing ratio (vmroh) for two altitude bands corresponding to the boundary layer and the upper troposphere.

For the boundary layer maps (figure 13), weak negative correlations persists for both models in most regions apart from oceanic regions associated with high water content low clouds such as the southern oceans, North Atlantic and again off the western coasts of South America and Africa. South Africa and Australia have positive correlations in GEOSCCM which is likely anomalous as they are regions of particularly low cloudiness (thus incidental correlations may occur), whereas the southern oceans are flagged more in GEOSCCM due to its biases. Clt and OH correlations at the boundary layer favours the positions of clouds due to low $J(O^1D)$ rates at the boundary layer as a result of absorption and scattering overhead by ozone, air molecules and clouds.

On the other hand, for the upper troposphere (figure 14), the equatorial regions and tropics have strong positive correlations corresponding to an increase in $J(O^1D)$ actinic flux where the ozone column is the thinnest. This altitude band is also where most cloud tops reside which enhances actinic fluxes from scattering. Cloud water content begins to decrease at these altitudes and so clt and OH correlations become sensitive to any spikes in water content, shown by the strong positive correlations in the deep convective regions of Central Pacific and Southeast Asia in MESSy. The strong correlations over Australia and South Africa as well as the absence of strong correlations over Southeast Asia in GEOSCCM is surprising and the reasons for this is not known. Overall correlations between clt and vmroh are not drastically different for GEOSCCM compared to MESSy considering its biases, but many inexplicable differences are present.

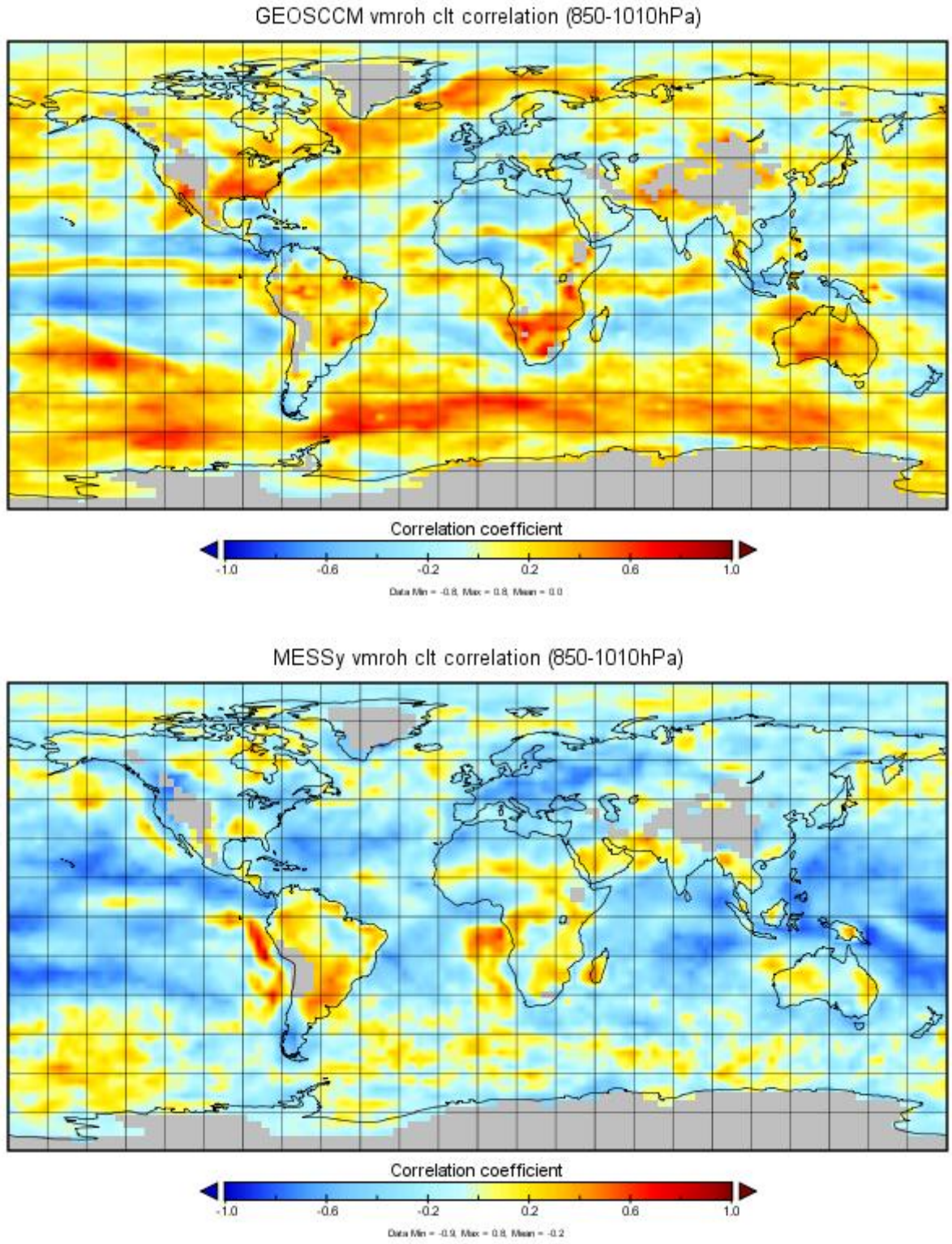

Figure 13 – Detrended correlations between total cloud fraction and OH molar mixing ratio for GEOSCCM (top) and MESSy (bottom) at the boundary layer (1010-850hPa). Grey grid-box values are a result of absence of values at particularly low pressures due to elevation over these regions.

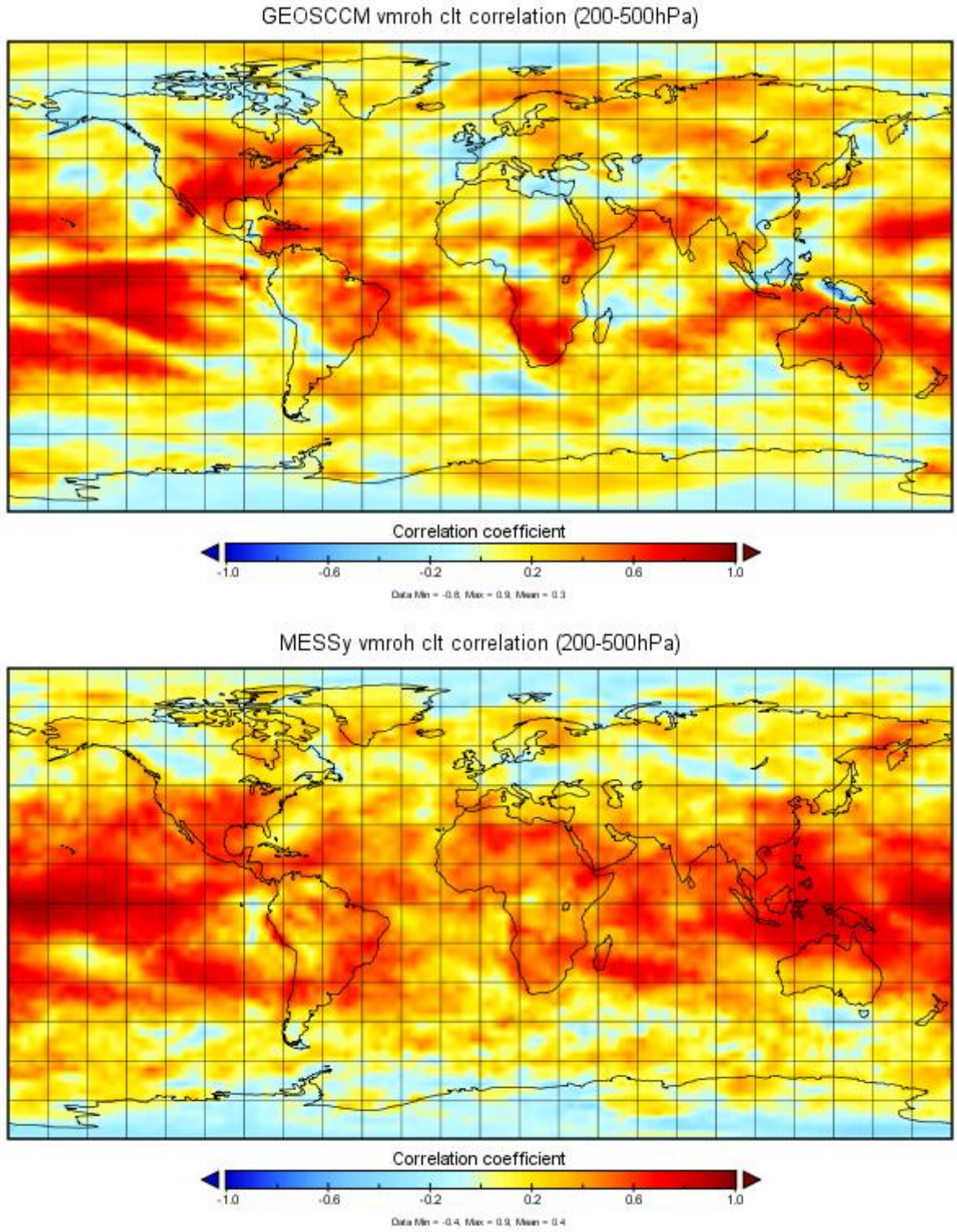

Figure 14 – Detrended correlations between total cloud fraction and OH molar mixing ratio for GEOSCCM (top) and MESSy (bottom) in the upper troposphere (500-200hPa).

7. Conclusion

Cloud and photolysis treatment was evaluated for two Chemistry Climate models participating in the Chemistry-Climate Model Initiative, namely GEOSCCM and MESSy. Analysis of the setup of the two models show substantial differences in the way the models solved for photolysis rates as well as implementation of clouds, cloud overlap and aerosol properties in their photolysis schemes. These differences in setup are a result of application of unique methods to save computation time and optimise properties of scattering particles in their atmospheres such that photolysis rates can be efficiently calculated along with the plethora of other dynamic and radiative processes that need to be simulated by these models.

Cloudiness as represented in GEOSCCM using the monthly total cloud fraction and monthly 3D cloud fraction variables contains significant low biases compared to observational data and MESSy. These cloud biases were shown not to affect rates of $J(NO_2)$, as both models were in close agreement over nearly all regions. Correlations remain as expected, negative at the surface below clouds due to attenuation of radiation and positive above due to backscattering, where deviations from these expected correlations were attributed to the different kinds of vertical cloud profiles over certain oceanic regions.

Biases in cloudiness over the Southern-hemisphere extratropical marine stratus region continue to persist in the current iteration of GEOSCCM. This considerably affects cloud and $J(NO_2)$ correlations, where they are positive throughout the atmosphere for MESSy as expected due to the optically thin shallow convective clouds that persist, whereas they are negative throughout the atmosphere for GEOSCCM likely due to an over-prescription of cloud optical depth as a result of the biases.

$J(O^1D)$ and cloud correlations seem to be more affected by the presence of prominent long-term trends as opposed to the low bias in cloudiness. Long term trend analysis of total cloud fraction, $J(O^1D)$ and ozone in India concluded that there is a significant increasing trend in ozone concentrations in the troposphere that is present in GEOSCCM but not in MESSy. One hypothesis is that the radiative effect of time-varying aerosols which is known to be omitted (in MESSy) in calculations of photolysis rates is causing a dimming of surface $J(O^1D)$ which contributes to feedbacks of ozone production. However the main conclusion is that omission of time-varying aerosols may result in omission of important tropospheric photochemistry processes and CCMs should include this if they are to claim the use of a fully interactive photolysis scheme. To confirm the hypothesis and conclusion, a plot of long term trends in surface layer aerosol emissions produced by the models would be needed which could be done in the future.

Total cloud fraction and OH correlations also remain largely unaffected by low cloud biases in GEOSCCM, however correlations seem inexplicably high over South Africa and Australia for reasons that are not known.

Overall, the results show that monthly cloud fraction variables in GEOSCCM at the specific spatial resolution used (2.5°/2° Lon/Lat) has issues representing clouds, however it is likely that cloud optical depths remain unaffected by this as seen by the correlations of clouds with photolysis rates being consistent with MESSy. If cloud optical depth data is produced for the two models in the future, then climatology maps could be produced to confirm this.

8. References

1. SPARC, 2013: SPARC Newsletter No. 40, January 2013, 68 pp., available at http://www.sparc-climate.org/newsletter.
2. Kong Fanyou and Qin Yu. The vertical transport of air pollutants by convective clouds. part i: A non-reactive cloud transport model. *Advances in Atmospheric Sciences*, 10(4):415–427, 1993.
3. Xuexi Tie, Renyi Zhang, Guy Brasseur, and Wenfang Lei. Global nox production by lightning. *Journal of Atmospheric Chemistry*, 43(1):61–74, 2002.
4. Xuexi Tie, Sasha Madronich, Stacy Walters, Renyi Zhang, Phil Rasch, and William Collins. Effect of clouds on photolysis and oxidants in the troposphere. *Journal of Geophysical Research: Atmospheres*, 108(D20):n/a–n/a, 2003. 4642.
5. Boucher, O., D. Randall, P. Artaxo, C. Bretherton, G. Feingold, P. Forster, V.-M. Kerminen, Y. Kondo, H. Liao, U. Lohmann, P. Rasch, S.K. Satheesh, S. Sherwood, B. Stevens and X.Y. Zhang, 2013: Clouds and Aerosols. In: Climate Change 2013: The Physical Science Basis. Contribution of Working Group I to the Fifth Assessment Report of the Intergovernmental Panel on Climate Change [Stocker, T.F., D. Qin, G.-K. Plattner, M. Tignor, S.K. Allen, J. Boschung, A. Nauels, Y. Xia, V. Bex and P.M. Midgley (eds.)]. Cambridge University Press, Cambridge, United Kingdom and New York, NY, USA.
6. Sasha Madronich. Tropospheric photochemistry and its response to uv changes. In Marie-Lise Chanin, editor, *The Role of the Stratosphere in Global Change*, volume 8 of *NATO ASI Series*, pages 437–461. Springer Berlin Heidelberg, 1993.
7. D. Jacob. *Introduction to Atmospheric Chemistry*. Princeton University Press, 1999.
8. Oliver Wild, Xin Zhu, and MichaelJ. Prather. Fast-j: Accurate simulation of in and below-cloud phtolysis in tropospheric chemical models. *Journal of Atmospheric Chemistry*, 37(3):245–282, 2000.
9. Hongyu Liu, James H Crawford, Robert B Pierce, Peter Norris, Steven E Platnick, Gao Chen, Jennifer A Logan, Robert M Yantosca, Mat J Evans, Chieko Kittaka, et al. Radiative effect of clouds on tropospheric chemistry in a global three-dimensional chemical transport model. *Journal of Geophysical Research: Atmospheres (1984–2012)*, 111(D20), 2006.
10. "Cloud Optical Thickness — GES DISC - Goddard Earth Sciences Data And Information Services Center". *Disc.sci.gsfc.nasa.gov*. N.p., 2016. Web. 24 Apr. 2016.
11. Morgenstern, O., et al. (2010), Review of the formulation of present-generation stratospheric chemistry-climate models and associated external forcings, J. Geophys. Res., 115, D00M02, doi:10.1029/2009JD013728.
12. Telford, P. J., Abraham, N. L., Archibald, A. T., Braesicke, P., Dalvi, M., Morgenstern, O., O'Connor, F. M., Richards, N. A. D., and Pyle, J. A.: Implementation of the Fast-JX Photolysis scheme (v6.4) into the UKCA component of the MetUM chemistry-climate model (v7.3), Geosci. Model Dev., 6, 161-177, doi:10.5194/gmd-6-161-2013, 2013.
13. Landgraf, J. and Crutzen, P. J.: An efficient method for online calculations of photolysis and heating rates, J. Atmos. Sci., 55, 863–878, 1998

14. Sander, R., Jöckel, P., Kirner, O., Kunert, A. T., Landgraf, J., and Pozzer, A.: The photolysis module JVAL-14, compatible with the MESSy standard, and the JVal PreProcessor (JVPP), Geosci. Model Dev., 7, 2653-2662, doi:10.5194/gmd-7-2653-2014, 2014.
15. Zdunkowski, W. G., Welch, R. M., and Korb, G.: An investigation of the structure of typical two-stream-methods for the calculation of solar fluxes and heating rates in clouds, Beitr. Phys. Atmos., 53, 147–166, 1980.
16. Bian, H., and M. J. Prather (2002), Fast-J2: Accurate simulation of stratospheric photolysis in global chemical models, J. Atmos. Chem., 41, 281 – 296.
17. Voulgarakis, A., Savage, N. H., Wild, O., Carver, G. D., Clemitshaw, K. C., and Pyle, J. A.: Upgrading photolysis in the p-TOMCAT CTM: model evaluation and assessment of the role of clouds, Geosci. Model Dev., 2, 59-72, doi:10.5194/gmd-2-59-2009, 2009.
18. Neu, J. L., M. J. Prather, and J. E. Penner (2007), Global atmospheric chemistry: Integrating over fractional cloud cover, J. Geophys. Res., 112, D11306, doi:10.1029/2006JD008007.
19. Feng, Y., J. E. Penner, S. Sillman, and X. Liu (2004), Effects of cloud overlap in photochemical models,J. Geophys. Res., 109, D04310, doi:10.1029/2003JD004040.
20. Roeckner, E., Bäuml, G., Bonaventura, L., Brokopf, R., Esch, M., Giorgetta, M., Hagemann, S., Kirchner, I., Kornblueh, L.,Manzini, E., Rhodin, A., Schlese, U., Schulzweida, U. & Tompkins, A. ´ (2003). The atmospheric general circulation model ECHAM 5. PART I: Model description (Eds.) Report / MPI für Meteorologie, 349
21. Stevens, B., et al. (2013), Atmospheric component of the MPI-M Earth System Model: ECHAM6, J. Adv. Model. Earth Syst., 5, 146–172, doi:10.1002/jame.20015.
22. Oman, L. D., and A. R. Douglass (2014), Improvements in total column ozone in GEOSCCM and comparisons with a new ozone-depleting substances scenario, J. Geophys. Res. Atmos., 119,5613–5624, doi:10.1002/2014JD021590.
23. Rossow, W. B., and R. A. Schiffer, 1999: Advances in understanding clouds from ISCCP. *Bull. Amer. Meteor. Soc.*,80, 2261–2287
24. Voulgarakis, A., Wild, O., Savage, N. H., Carver, G. D., and Pyle, J. A.: Clouds, photolysis and regional tropospheric ozone budgets, Atmos. Chem. Phys., 9, 8235-8246, doi:10.5194/acp-9-8235-2009, 2009.
25. Oman, L. D., and A. R. Douglass (2014), Improvements in total column ozone in GEOSCCM and comparisons with a new ozone-depleting substances scenario, J. Geophys. Res. Atmos., 119,5613–5624, doi:10.1002/2014JD021590.

Appendix A – Region location and definitions

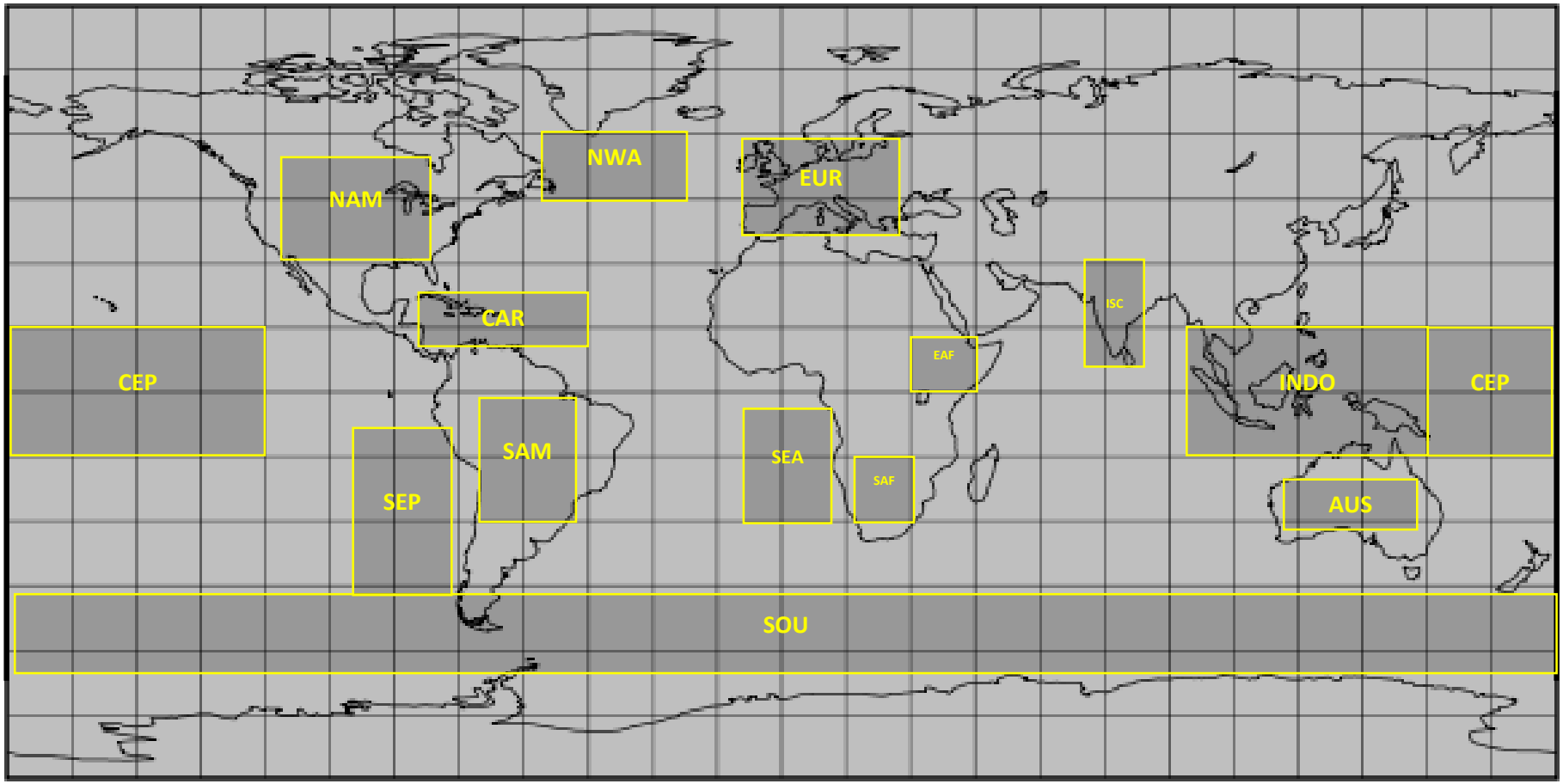

Region name	Syntax	Lat min	Lat max	Lon min	Lon max
Europe	EUR	37	59	0	28
Eastern Africa	EAF	0	13	30	45
Southern Africa	SAF	-30	-15	17	31
Indian Subcontinent	ISC	6	30	71	84
Indonesia	INDO	-15	15	95	150
Australia	AUS	-32	20	117	148
Southern Ocean	SOU	-66	-47	0	360
Central Equatorial Pacific	CEP	-15	15	150	240
Southeast Pacific	SEP	-47	-8	261	284
South America	SAM	-30	-1	290	312
Caribbean	CAR	11	23	276	315
North America	NAM	30	53	244	278
Northwest Atlantic	NWA	45	60	304	338
Southeast Atlantic	SEA	-30	-4	0	12

Appendix B – 3D cloud profile plots using 'cl' variable (GEOSCM:Left, MESSy:right)

(Note – Y axis increases with pressure from TOA to boundary layer)

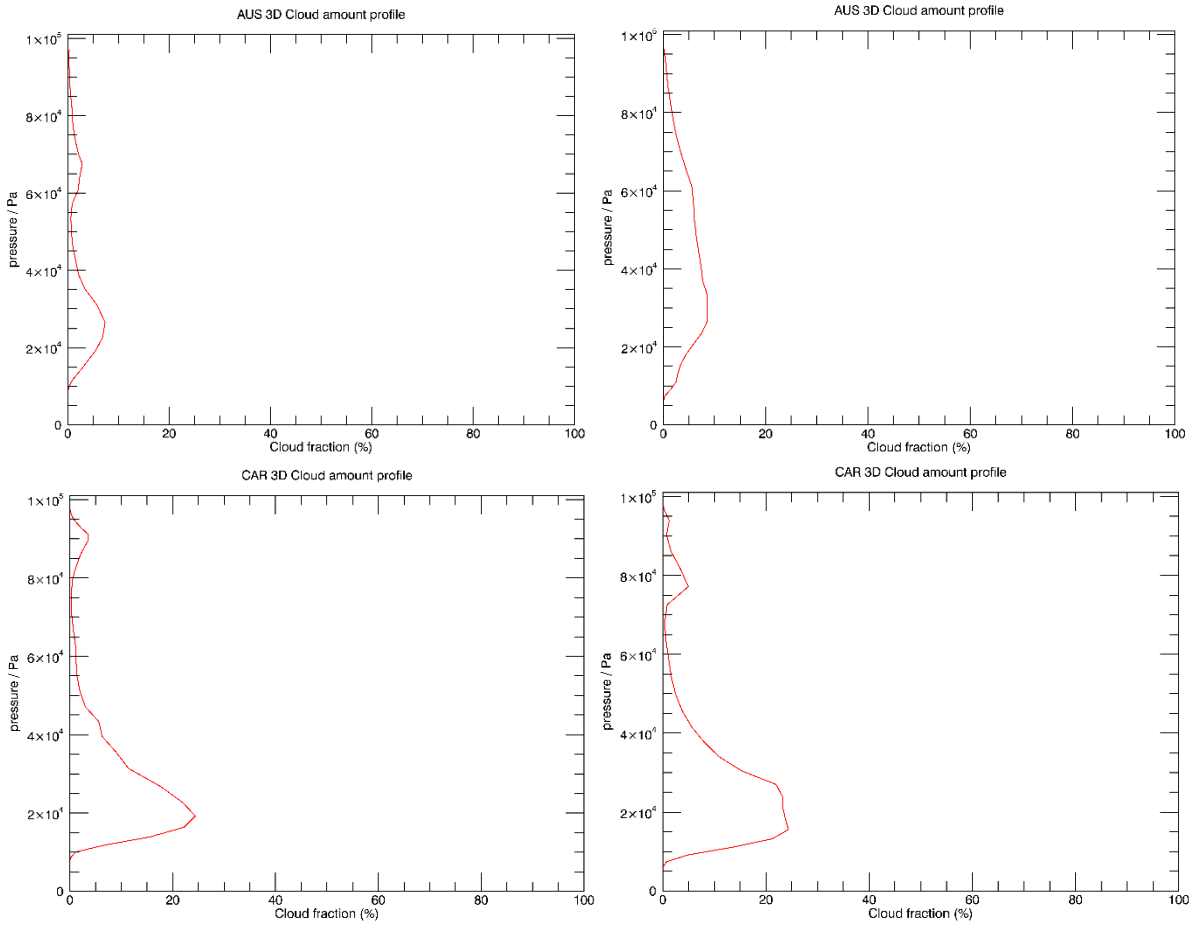

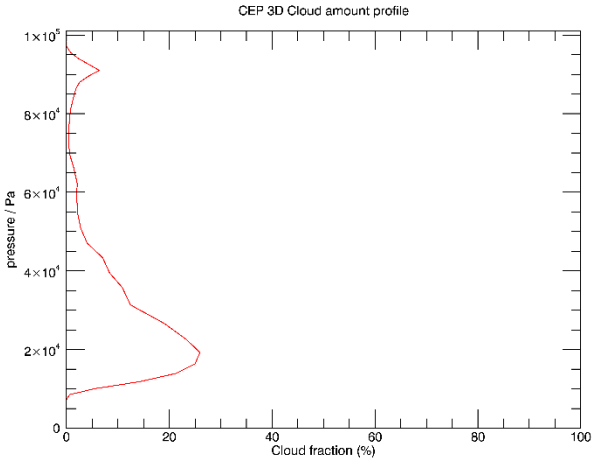
CEP 3D Cloud amount profile
pressure / Pa
Cloud fraction (%)

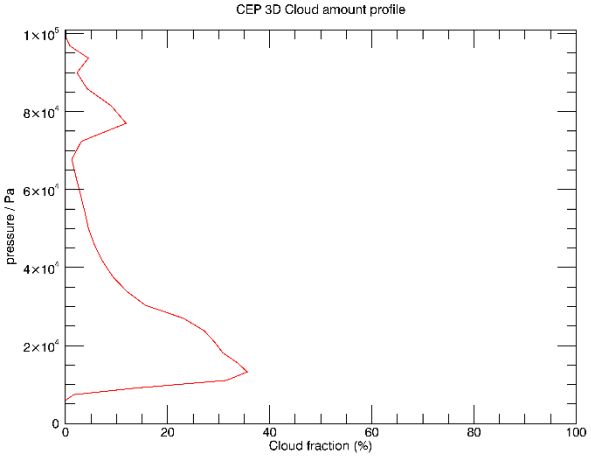
CEP 3D Cloud amount profile
pressure / Pa
Cloud fraction (%)

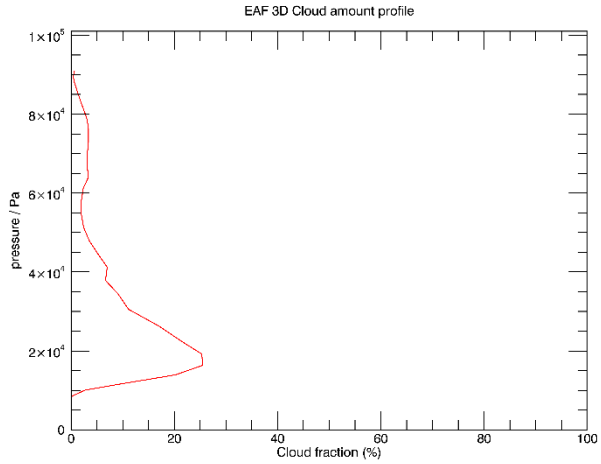
EAF 3D Cloud amount profile
pressure / Pa
Cloud fraction (%)

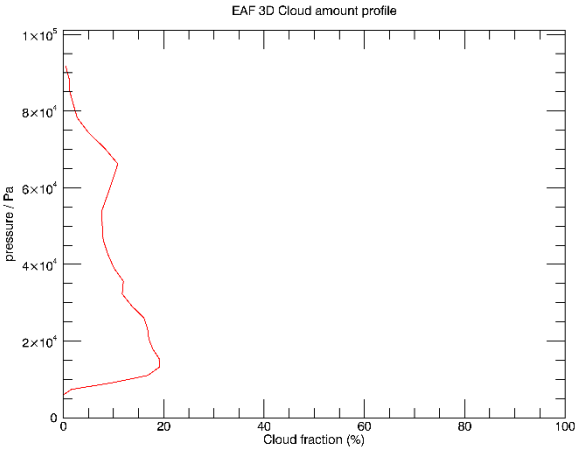
EAF 3D Cloud amount profile
pressure / Pa
Cloud fraction (%)

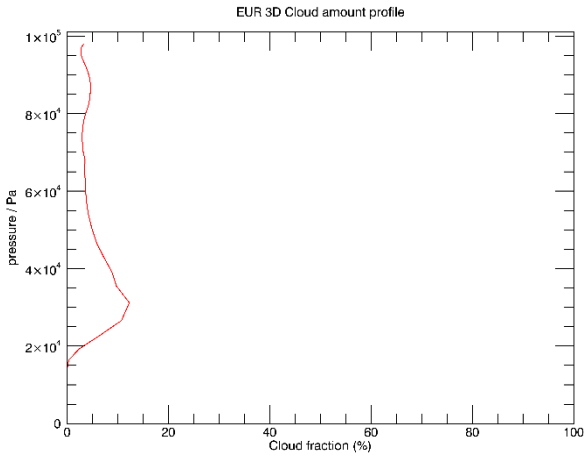
EUR 3D Cloud amount profile
pressure / Pa
Cloud fraction (%)

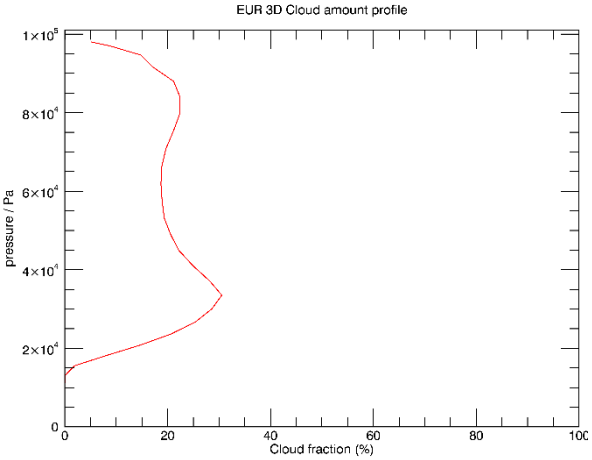
EUR 3D Cloud amount profile
pressure / Pa
Cloud fraction (%)

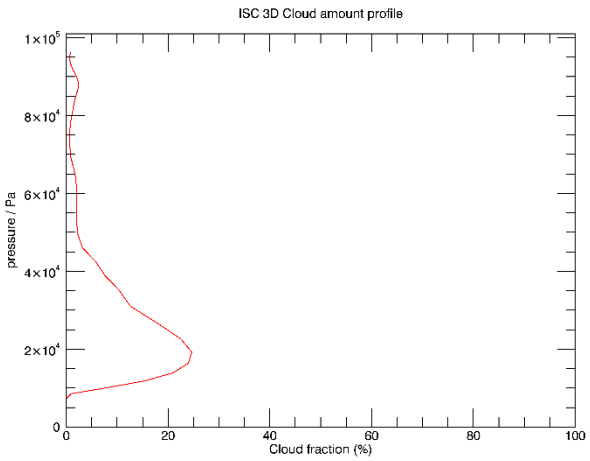
ISC 3D Cloud amount profile
pressure / Pa
Cloud fraction (%)

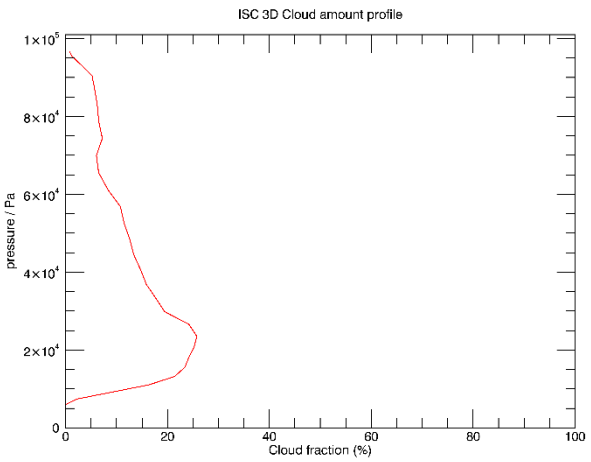
ISC 3D Cloud amount profile
pressure / Pa
Cloud fraction (%)

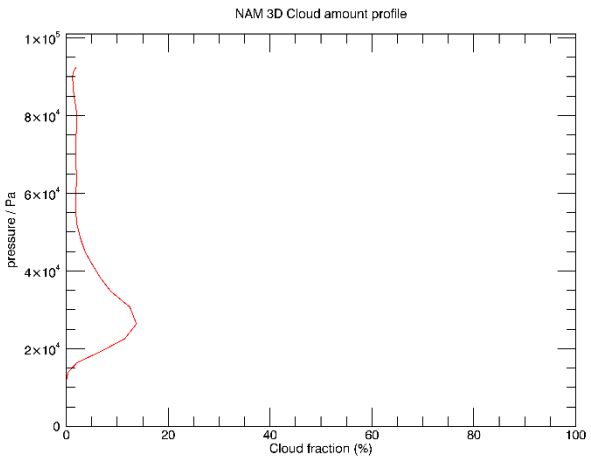
NAM 3D Cloud amount profile
pressure / Pa
Cloud fraction (%)

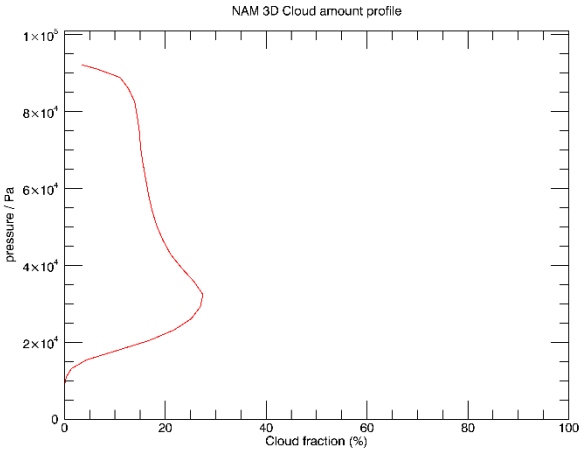
NAM 3D Cloud amount profile
pressure / Pa
Cloud fraction (%)

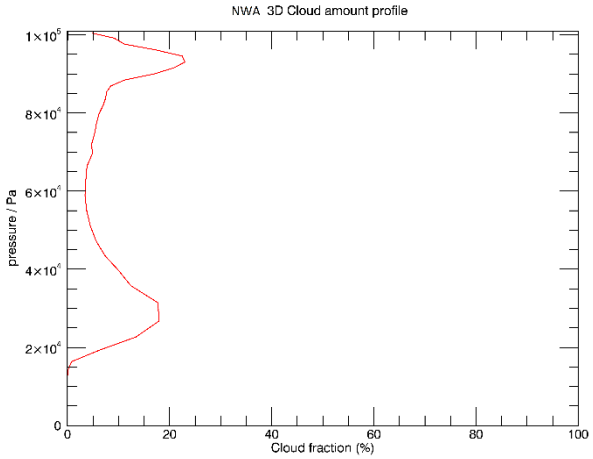
NWA 3D Cloud amount profile
pressure / Pa
Cloud fraction (%)

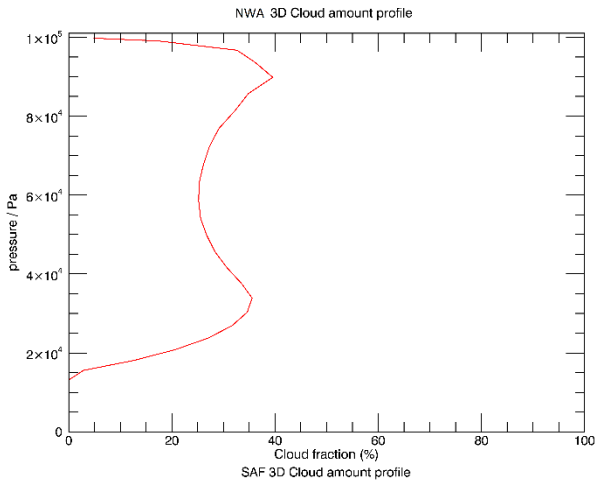
NWA 3D Cloud amount profile
pressure / Pa
Cloud fraction (%)

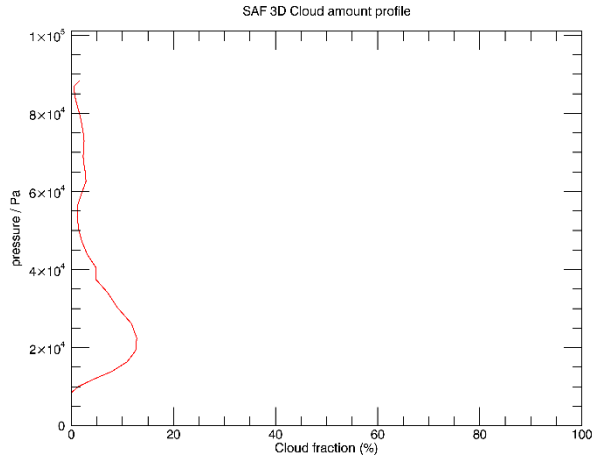
SAF 3D Cloud amount profile
pressure / Pa
Cloud fraction (%)

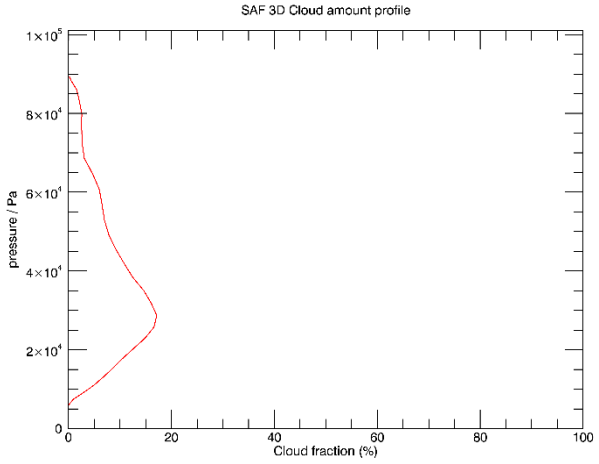
SAF 3D Cloud amount profile
pressure / Pa
Cloud fraction (%)

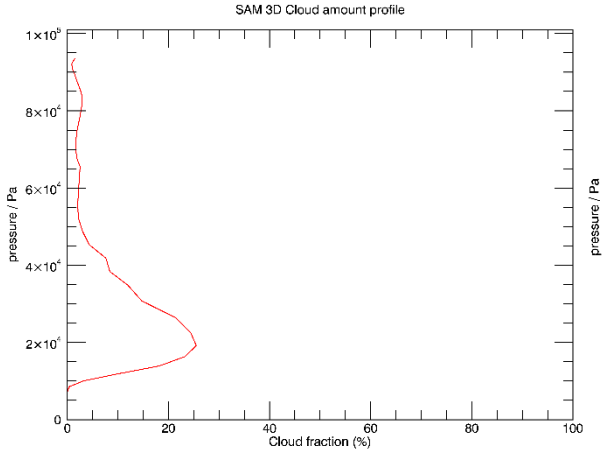
SAM 3D Cloud amount profile
pressure / Pa
Cloud fraction (%)

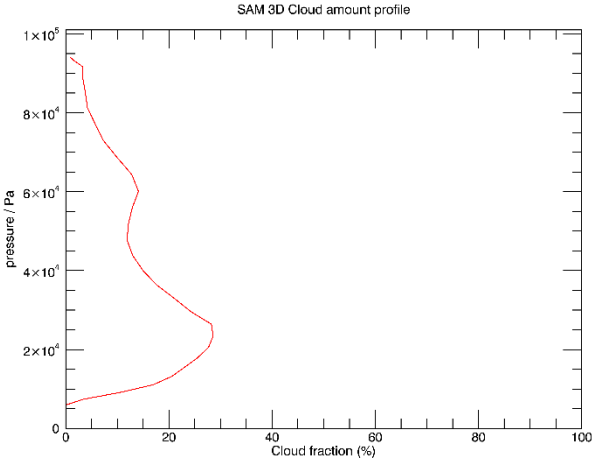
SAM 3D Cloud amount profile
pressure / Pa
Cloud fraction (%)

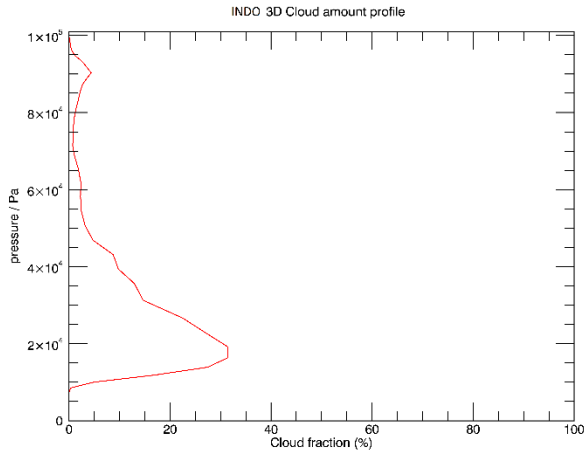
INDO 3D Cloud amount profile
pressure / Pa
Cloud fraction (%)

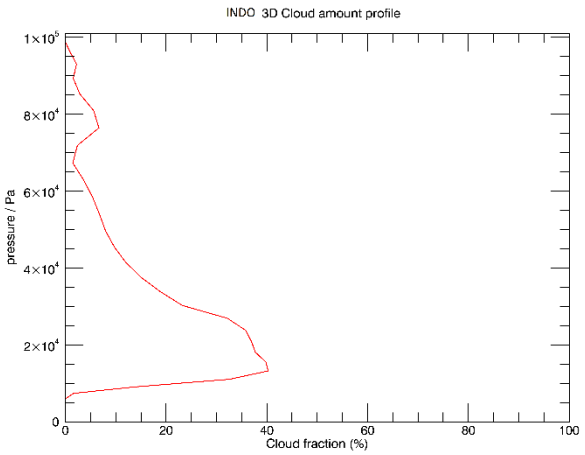
INDO 3D Cloud amount profile
pressure / Pa
Cloud fraction (%)

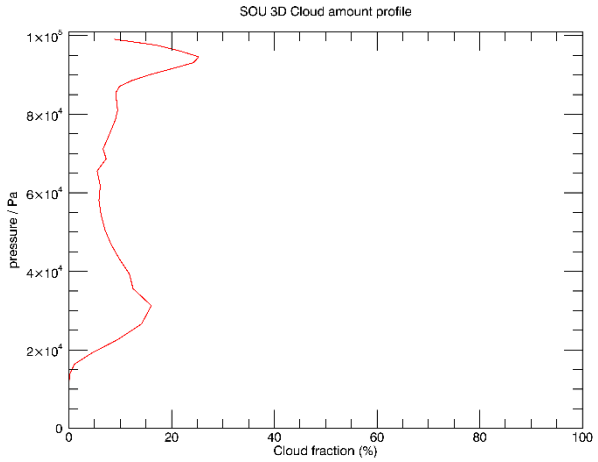
SOU 3D Cloud amount profile
pressure / Pa
Cloud fraction (%)

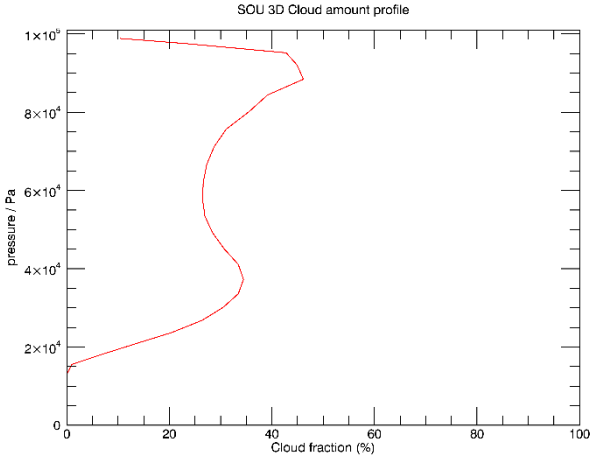
SOU 3D Cloud amount profile
pressure / Pa
Cloud fraction (%)

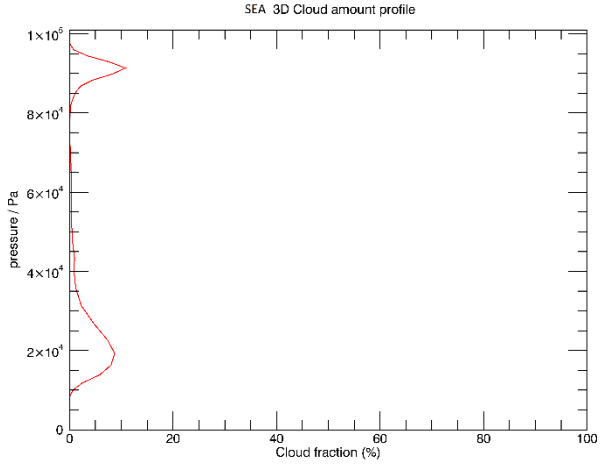
SEA 3D Cloud amount profile
pressure / Pa
Cloud fraction (%)

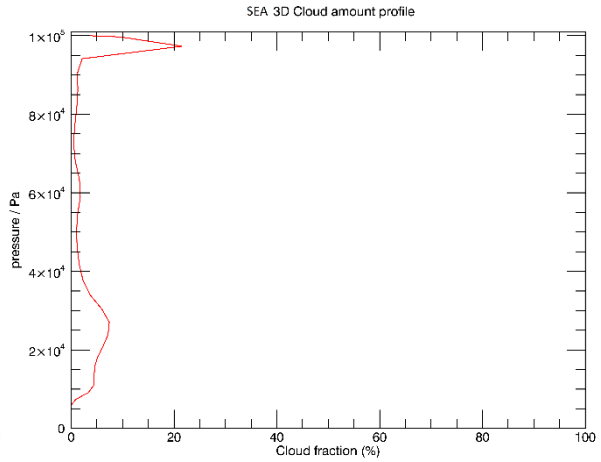
SEA 3D Cloud amount profile
pressure / Pa
Cloud fraction (%)

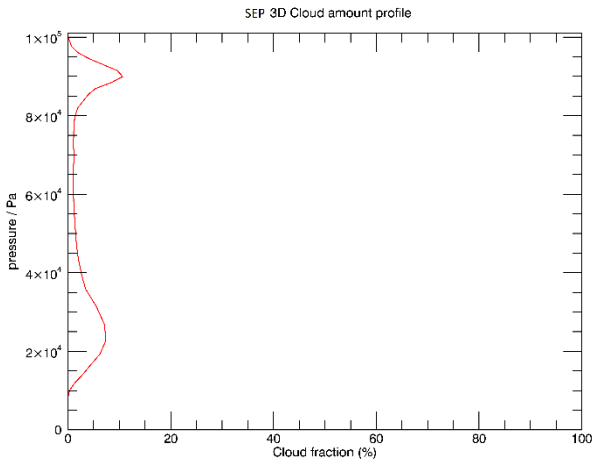
SEP 3D Cloud amount profile
pressure / Pa
Cloud fraction (%)

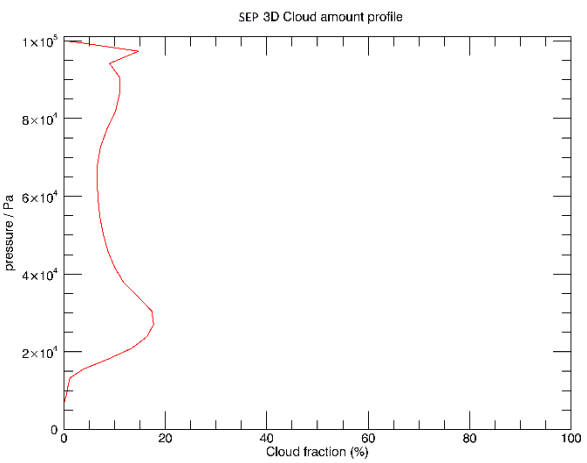
SEP 3D Cloud amount profile
pressure / Pa
Cloud fraction (%)